DISSERTATION

TAZ-regulated RUNX2 signaling drives pulmonary artery calcification in pulmonary hypertension due to left heart disease

TAZ-reguliertes RUNX2-Signaling fördert die Verkalkung der Lungenarterie bei pulmonaler Hypertonie aufgrund von Linksherzerkrankungen

zur Erlangung des akademischen Grades
Doctor medicinae (Dr. med.)

vorgelegt der Medizinischen Fakultät
Charité – Universitätsmedizin Berlin

von

Shaofei, Liu

Erstbetreuung: Professor Dr.med. Wolfgang M., Kuebler

Datum der Promotion: 29.11.2024

Table of Contents

List of Tables

List of Figures

List of Abbreviations

AB	Amido black
AoB	Supracoronary aortic banding
BW	Body weight
CBF-α1	Core-binding factor subunit α1
CHX	Cycloheximide
CI	Cardiac index
Co-IP	Co-immunoprecipitation
DAPI	4′,6-diamidino-2-phenylindole
DMEM	Dulbecco’s modified eagle’s medium
eGFR	Estimated glomerular filtration rate
FBS	Fetal bovine serum
GO	Gene ontology
IP	Immunoprecipitation
LV	Left ventricular
LV+S	LV and septum
LVSP	Left ventricular systolic pressure
mPAP	Mean pulmonary artery pressure
PA	Pulmonary artery
PA RS	Pulmonary arterial radial strain
PAAT	Pulmonary artery acceleration time
PAH	Pulmonary arterial hypertension
PASMC	Pulmonary artery smooth muscle cells
PAWP	Pulmonary artery wedge pressure
PFA	Paraformaldehyde

PH	Pulmonary hypertension
PH-LHD	Pulmonary hypertension due to left heart disease
PVDF	Polyvinylidene difluoride
RHC	Right heart catheterization
RIPA	Radioimmunoprecipitation assay
RT-qPCR	Real-time quantitative polymerase chain reaction
RUNX2	Runt-related transcription factor 2
RV	Right ventricular
RVEF	Right ventricular ejection fraction
RVSP	Right ventricular systolic pressure
SD	Sprague-Dawley
SMC	Smooth muscle cells
TAPSE	Tricuspid annular plane systolic excursion
TAZ	Transcriptional coactivator with PDZ-binding motif
TBST	Tris-buffered saline with 0.1% Tween-20
TEAD	TEA domain
TGF-β	Transforming growth factor-β
VP	Verteporfin
YAP	Yes-associated protein

Abstract

Pulmonary hypertension (PH) due to left heart disease (PH-LHD) is a prevalent and prognostically unfavourable form of PH. Vascular calcification, a common characteristic of chronic vascular disease processes, is associated with increased vascular stiffness in aging and cardiovascular diseases such as hypertension, diabetes mellitus, and atherosclerosis, but has so far not been investigated in the context of PH-LHD. The present study aimed to address the relevance of vascular calcification in PH-LHD, explore its potential pathophysiological implications, and uncover the underlying mechanisms involved. Through gene ontology (GO) term analysis, we detected a significant enrichment of genes associated with ossification (GO:0001503) and osteoblast differentiation (GO:0001649). Specifically, we found the expression of the master transcription factor of osteogenesis, runt-related transcription factor 2 (RUNX2), increased in the pulmonary artery (PA) of PH-LHD patients and in the lungs of rats with supracoronary aortic banding (AoB), a relevant animal model of PH-LHD. PA calcification was evident in both PH-LHD patients and AoB rats. Further investigations revealed the upregulation and nuclear translocation of RUNX2 and its regulation by the HIPPO pathway transcriptional coactivator with PDZ-binding motif (TAZ) in pulmonary arterial smooth muscle cells (PASMC) from PH-LHD patients, AoB rats, and in PASMC stimulated with transforming growth factor-β (TGF-β), a known driver of lung vascular remodeling. Co-immunoprecipitation studies demonstrated an increased interaction between RUNX2 and TAZ in TGF-β-treated PASMC. Inhibition or siRNA-mediated knockdown of TAZ led to a decrease in RUNX2 abundance due to accelerated protein degradation rather than reduced synthesis. Inhibition of either TAZ or RUNX2 attenuated PA calcification, distal lung vascular remodeling, and the development of PH in AoB rats. As such, our findings identify the TAZ-RUNX2 axis as a potential therapeutic target for the treatment of PH-LHD.

Zusammenfassung

Pulmonale Hypertonie (PH) aufgrund von Linksherzerkrankungen (PH-LHD) ist eine weit verbreitete und prognostisch ungünstige Form der PH. Gefäßverkalkungen, ein häufiges Merkmal chronischer Gefäßerkrankungen, das mit einer erhöhten Gefäßsteifigkeit im Alter und bei kardiovaskulären Erkrankungen wie Hypertonie, Diabetes mellitus und Arteriosklerose verbunden ist, wurden bisher nicht dezidiert im Zusammenhang mit PH-LHD untersucht. Die vorliegende Studie zielt darauf ab, die Relevanz von Gefäßverkalkungen bei PH-LHD zu untersuchen, ihre potenziellen pathophysiologischen Auswirkungen zu erkunden und die zugrunde liegenden Mechanismen aufzudecken. Durch die Analyse von Genontologie-Termini (GO-Termini) konnten wir bei PH-LHD eine signifikante Anreicherung von Genen identifizieren, die mit Ossifizierung (GO:0001503) und der Differenzierung von Osteoblasten (GO:0001649) assoziiert sind. Insbesondere wurde eine erhöhte Expression des Master-Transkriptionsfaktors der Osteogenese, Runt-related Transcription Factor 2 (RUNX2), in den Lungenarterien (PA) von PH-LHD Patienten und den Lungen von Ratten mit suprakoronarem Aortenbanding (AoB), einem relevanten Tiermodell der PH-LHD, beobachtet. PA-Verkalkungen waren histologisch sowohl bei PH-LHD Patienten als auch bei AoB-Ratten deutlich erkennbar. Weitere Untersuchungen zeigten die Hochregulation und nukleäre Translokation von RUNX2 sowie seine Regulation durch den Co-Aktivator des HIPPO-Signalweges Transcriptional Coactivator with PDZ binding motif (TAZ) in glatten Muskelzellen der Lungenarterien (PASMC) bei PH-LHD-Patienten, AoB-Ratten und in PASMC, die mit *Transforming Growth Factor-β* (TGF-β) stimuliert wurden, einem bekannten Mediator des pulmonalvaskulären Gefäßumbaus. Co-Immunpräzipitationsstudien zeigten eine erhöhte Interaktion zwischen RUNX2 und TAZ in TGF-β behandelten PASMC. Hemmung oder siRNA-vermittelter Knockdown von TAZ führten zu einer Abnahme des Proteins RUNX2, die auf einen beschleunigten Proteinabbau, nicht hingegegen auf eine verringerte Synthese zurückgeführt werden konnte. Die Hemmung von TAZ oder RUNX2 minderte die PA-Verkalkung, den Umbauder peripheren Lungengefäße und die Entwicklung einer PH bei AoB-Ratten. Unsere Befunde identifizieren somit die gezielte Beeinflussung der TAZ-RUNX2-Achse als eine potenzielle therapeutische Strategie für die Behandlung der PH-LHD.

1. Introduction

1.1 Pulmonary hypertension due to left heart disease

Pulmonary hypertension (PH) is a progressive vascular disease affecting the heart and the lungs. It is characterized by an increase in mean pulmonary artery pressure (mPAP) exceeding 20 mmHg at rest [1]. Over time, this condition can ultimately lead to right ventricular failure and eventually death. Pulmonary hypertension due to left heart disease (PH-LHD) is the most common type of PH [2]. Despite its prevalence, our current understanding of the underlying mechanisms driving pulmonary vascular remodeling in PH-LHD is rudimentary at best [3], and at present, there are no established therapeutic strategies for the treatment of PH-LHD.

1.2 Vascular calcification

Vascular calcification is a hallmark of vascular aging and systemic cardiovascular diseases [4], and commonly associated with conditions such as diabetes mellitus [5], atherosclerosis [6], and renal dysfunction [7]. At the cellular level, vascular calcification is primarily driven by the transdifferentiation of vascular smooth muscle cells (SMC) into osteoblast-like cells, and prompted by pathological hemodynamics, metabolic, or inflammatory stimuli [8-10]. In terms of molecular mechanisms, runt-related transcription factor 2 (RUNX2), also referred to as core-binding factor subunit α1 (CBF-α1) [11], was initially recognized as a pivotal transcription factor in osteoblast differentiation. Recent studies, however, have highlighted its crucial role also as a regulatory factor in vascular calcification. As such, RUNX2 drives the osteogenic reprogramming of SMC, leading to the deposition of calcium in the arterial wall [12, 13].

The occurrence of vascular calcification varies between diverse blood vessel types, the specific underlying disease, and the affected layer of the vascular wall [14]. While the significance and underlying mechanisms of vascular calcification in the aorta or coronary arteries have been extensively studied, the understanding of its relevance in the pulmonary vasculature remains limited. In a seminal study conducted in 2016, Ruffenach and colleagues were the first to detect calcified lesions in the pulmonary artery (PA) of indi-

viduals diagnosed with pulmonary arterial hypertension (PAH) [15]. As such, the presence and impact of vascular calcification in PH-LHD, its potential contribution to disease progression and its underlying regulatory mechanisms have yet to be explored.

1.3 The interaction between RUNX2 and TAZ in osteoblastogenesis

In the context of vascular calcification, the transformation of smooth muscle cells (SMC) into an osteogenic phenotype is predominantly driven by RUNX2 [13], a master regulator of skeletal development and osteogenic differentiation [16]. Upon activation, RUNX2 translocates from the cytosol to the nucleus, where it exerts its function by promoting the expression of osteogenic genes [15].

In PH-LHD, remodeling of the lung vasculature is primarily driven by increased mechanical forces that exert pressure (and therefore, tangential force and stretch) on the walls of pulmonary vessels. These mechanical forces are detected by mechanosensitive ion channels, cell-cell contacts, and signaling pathways within the lung vascular cells that in turn drive vascular remodeling processes. Of late, the HIPPO signaling pathway, which involves the kinases LATS1/2 and the transcriptional co-activators Yes-associated protein (YAP) and transcriptional coactivator with PDZ-binding motif (TAZ), has emerged as a key factor in both lung vascular mechanosensation [17] as well as the remodeling processes involved in PAH [18, 19].

Importantly, in osteoblastogenesis, TAZ has been shown to synergize with RUNX2 by forming a complex of master transcription factors [20]. As such, TAZ signaling emerges as a promising candidate that may initiate or amplify RUNX2-mediated osteogenic calcification in response to mechanical stress as is present in PH-LHD. In parallel to mechanical stress, TAZ signaling is also activated by transforming growth factor-β (TGF-β) [21], a major regulator of lung vascular remodeling in PAH [22-24] that is also elevated in lungs and serum of animal models of PH-LHD [25, 26]. Hence, TGF-β signaling could act as an additional stimulus of mechanical stress for TAZ/RUNX2 signaling in PH-LHD and may potentially be utilized as an *in vitro* model to investigate their interaction.

1.4 Aims of the study

In the present study, we aimed to investigate the development of PA calcification in PH-LHD and to examine its role in the development and/or progression of PH. At the mechanistic level, we propose that RUNX2 drives the osteogenic calcification of PASMC in PH-LHD, and that RUNX2 may be activated at least in part via its interaction with the mechanosensitive transcriptional co-activator TAZ and via stimulation by TGF-β (**Fig. 1**). To address these hypotheses, we i) assessed vascular calcification in PA and lung tissue in an established rat model of PH-LHD [27-29], ii) characterized PA calcification in tissue samples obtained from PH-LHD patients and healthy-heart donors, iii) performed mechanistic analyses in cultured human PASMC, and iv) conducted interventional studies in PH-LHD rats.

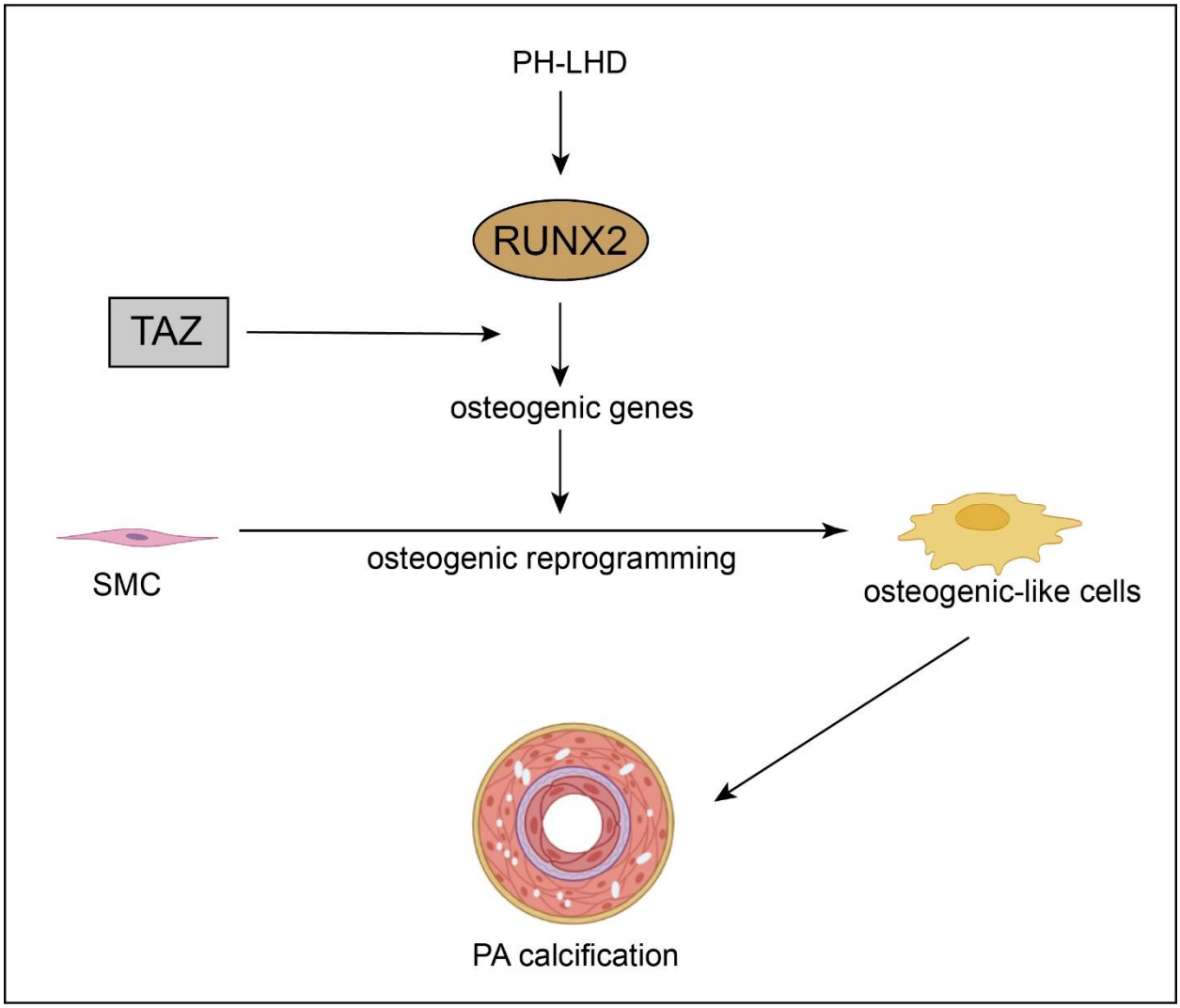

Figure 1. Schematic illustration of the central hypothesis.

In the present work, we probed the following new hypothesis with respect to lung vascular remodeling in PH-LHD: In PH-LHD, the transcription factor RUNX2 drives osteogenic differentiation of PASMC characterized by the expression of osteogenic genes and progressive calcification of PA. The HIPPO transcriptional co-activator TAZ amplifies this process by its interaction with the osteogenic transcription factor RUNX2.

2. Methods

2.1 Human patient samples

Human tissue and blood were collected following approval by the Ethics Committee of the Charité-Universitätsmedizin Berlin (EA4/035/18 and EA1/134/23) and with the informed consent of the patients. Specimens from the pulmonary trunk (PA samples) were collected at the Deutsches Herzzentrum der Charité (DZHC) during orthotopic heart transplantation from healthy-heart donors (control, n=20) to patients with PH-LHD (n=23) when the length of the PA was adjusted prior to surgical anastomosis. Diagnosis of PH-LHD was confirmed by right heart catheterization (RHC) within 6 months prior to transplantation as a mean pulmonary artery pressure (mPAP) > 20 mmHg and a pulmonary artery wedge pressure (PAWP) > 15 mmHg according to current guidelines [1]. The clinical characteristics of human subjects are summarized in **Table 1**. Blood was drawn from PH-LHD patients and healthy volunteers (n=4, age: 43±8 years) in BD Vacutainer Plastic K2EDTA tubes (Fisher Scientific). Cells were removed from the plasma by centrifugation for 10 min at 4,000 rpm using a refrigerated (4°C) centrifuge. The supernatant (plasma) was collected and stored at -80°C. The estimated glomerular filtration (eGFR) rate was calculated from plasma creatinine according to the 2021 CKD-EPI Equation [30].

Table 1. Clinical characteristics of patients with pulmonary hypertension due to left heart disease (PH-LHD) and healthy-heart donors (control)

	control (n = 20)	**PH-LHD (n = 23)**
Age, years	42.3 ± 15.2	52.3 ± 12.1
Sex, female, n (%)	6 (30.0)	7 (30.4)
mPAP, mmHg	n.d.	30.7 ± 8.9
PAWP, mmHg	n.d.	22.1 ± 7.0
CI, L/min	n.d.	2.6 ± 1.1
eGFR, mL/min/1.73m^2		male: 68.4 ± 29.1 female: 67.2 ± 20.6

Definition of abbreviations: mPAP, mean pulmonary artery pressure; PAWP, pulmonary artery wedge pressure; CI, cardiac index; eGFR, estimated glomerular filtration rate (normal range: 90 to 120 mL/min/1.73 m^2); n.d., not determined. Values are given as mean ± SD.

2.2 Animal experiments

2.2.1 Rat model of PH-LHD induced by supracoronary aortic banding (AoB)

Procedures were approved by the local governmental animal care and use committee of the German State Office for Health and Social Affairs (Landesamt für Gesundheit und Soziales, LaGeSO, Berlin; protocol no. G0030/18; approved on 11.06.2018) and followed the "Guide for the Care and Use of Laboratory Animals" (Institute of Laboratory Animal Resources, 8th edition 2011). PH-LHD was induced in male Sprague-Dawley (SD) rats (approx. 100 g body weight (BW)) in an established model of AoB as previously described [27, 31]. In brief, rats were injected with carprofen (5 mg/kg BW; CP-Pharma, Germany) intraperitoneally (i.p.) for analgesia 30 min prior to surgery, and then anesthetized by intraperitoneal (i.p.) injection of ketamine (87 mg/kg BW) and xylazine (13 mg/kg BW; both CP-Pharma, Germany). Bepanthen cream (Bayer, Germany) was used for eye protection. Rats were tracheotomized, intubated, and mechanically ventilated at a respiratory rate of 90 breaths/min with a tidal volume (Vt) of 8.5 mL/kg BW. The thorax was opened at the second left intercostal space to expose the ascending aorta, and a metal titanium clip (Hemoclip®, Weck Closure System, Research Triangle Park, NC) with a preset internal diameter of 0.8 mm was placed across the ascending aorta. For the first 7 days post-surgery, rats received daily i.p. injections of carprofen (5 mg/kg BW; CP-Pharma, Germany) and amoxicillin (Ratiopharm, Germany) via the drinking water for postoperative analgesia and antisepsis, respectively. Rats in the sham group underwent the same surgical procedure and post-operative treatment, yet without clipping of the aorta. In subgroups of experiments, rats were treated in a randomized manner with either the RUNX2 inhibitor CADD522 (10 mg/kg BW; Med Chem Express), the YAP/TAZ inhibitor verteporfin (10 mg/kg BW; Med Chem Express) or vehicle DMSO, each given i.p. twice per week starting at post-operative week 4 for 6 weeks.

2.2.2 Echocardiography, hemodynamic assessment, and tissue collection

Ultrasonographic assessment of the right and left heart and of pulmonary hemodynamics were performed at the Core facility of the Charité CrossOver as described previously [32]. In brief, transthoracic echocardiography was performed on a VisualSonics Vevo 3100 ultrasound system (FUJIFILM VisualSonics, Amsterdam, Netherlands) using an MX-250 transducer. Rats were anesthetized with 1.5% isoflurane (CP-Pharma, Germany), then placed in a supine position on a heating pad with the legs connected to electrocardiographic electrodes for heart rate monitoring. The chest area was shaved for echocardiographic access. From M-mode recordings of the apical four chamber views, tricuspid annular plane systolic excursion (TAPSE) was determined with the M-mode cursor oriented to the junction of the tricuspid valve plane and the right ventricular (RV) free wall. Pulmonary artery acceleration time (PAAT) was measured from the pulsed-wave Doppler flow velocity profile of the RV outflow tract in the parasternal short-axis view and was defined as the time interval from the onset to the maximal velocity of forward flow. Right ventricular ejection fraction (RVEF) was determined from M-mode tracings of the parasternal long-axis view above the aortic root. Pulmonary arterial radial strain was calculated as PA RS = (DMax - DMin) / DMin, where DMax and DMin are the maximum and minimum PA diameters measured in the modified parasternal long axis view, respectively.

Within 48 hours after echocardiographic recordings, a comprehensive hemodynamic evaluation was performed as the endpoint measurement. In brief, rats were again anesthetized with ketamine (87 mg/kg BW) and xylazine (13 mg/kg BW). Following a median thoracotomy, cardiac catheterization was performed by direct introduction of a microtip Millar catheter connected to a PowerLab data acquisition system (MPVS-Ultra Single Segment Foundation System, AD Instruments) and LabChart 8 for Windows software through the apex of (first) the left and (second) the right ventricle, respectively. Notably, direct catheterization of the left ventricle via the vascular route is precluded by the aortic band in AoB animals.

Animals were then euthanized in accordance with animal welfare. Blood was collected by exsanguination via cardiac puncture. The left lung was fixed in 10% neutral buffered formalin for histological assessment, and the right lung was snap frozen in liquid nitrogen. For assessment of ventricular hypertrophy, the RV was carefully separated from the LV and septum (LV+S), and RV or LV+S weight was calculated relative to body weight (BW).

2.3 Isolation of primary PASMC from human PA, cell culture, and transfection

PASMC were isolated from PA samples collected from PH-LHD patients or healthy-heart donors, respectively. To this end, the endothelium was removed by gentle scraping with a scalpel blade, and the media was peeled away from the underlying adventitial layer. The medial explants were cut into approximately 1-2 mm^2 sections, transferred to T25 flasks with DMEM supplemented with 20% fetal bovine serum (FBS), penicillin (100 U/mL), and streptomycin (100 µg/mL) and allowed to adhere for 72 hours at 37°C and 5% CO_2. Once the cells adhered, PASMC were cultured in DMEM/F12 with 10% FBS, penicillin, and streptomycin until the cells had formed confluent monolayers. The purity of isolated primary human PASMC was analyzed by immunofluorescence staining for α-smooth muscle actin (α-SMA, Sigma-Aldrich A2547). Commercially available human PASMC were obtained from PromoCell (Heidelberg, Germany) and cultured in Smooth Muscle Cell Growth Medium 2 (C-22062, PromoCell). All cells were used at passages 4-8 for experiments.

For siRNA-based silencing of TAZ, pre-designed, commercially available siRNA sequences directed against human TAZ were purchased. To control for non-specific gene inhibition, a universal negative-control siRNA sequence was used (siScram). Human PASMC were transiently transfected for 72 hours with siTAZ (50 nMol/L, Santa Cruz, SC-38568) or siScram (50 nMol/L, Dharmacon, ON-TARGETplus Non-targeting Control Pool) using Lipofectamine 2000 Transfection Reagent (Thermo Fisher, 11668019). Effective knockdown was verified by western blotting.

2.4 Vascular remodeling and nuclear translocation of RUNX2 and TAZ

Formalin-fixed rat lungs were paraffin-embedded. Serial sections of 5 µm were cut, deparaffinized in xylene, and rehydrated in a graded ethanol series to PBS. Antigen retrieval was performed with Tris-EDTA (pH=9) in a microwave at 600°C for 10 min. To assess vascular remodeling, lung sections were stained with anti-α-SMA antibody (1:500), nuclei were counterstained with 4′,6-diamidino-2-phenylindole (DAPI, 1:1,000), and fluorescence staining was visualized by either a Zeiss transillumination microscope (Axioskop 40, Zeiss, Germany) or by confocal microscopy (Upright Spinning Disk confocal CSU-X, Nikon, Germany) for quantification of medial thickening in distal PA. Arterial wall thickness

(in %) was calculated as (external diameter − internal diameter)/external diameter × 100 as described [33].

For immunofluorescent imaging of the expression and nuclear translocation of RUNX2 and TAZ, OCT-frozen PA tissues from human samples were thawed at room temperature for 60 min and washed with PBS for 10 min prior to sectioning as described above. Rat lung sections were deparaffinized as described before. All slides were blocked with PBTB (0.2% Triton X-100, 0.2% bovine serum albumin, 5% normal goat serum, and 0.05% sodium azide in 1xPBS) for 60 min. Double immunofluorescence staining was performed with primary antibodies against RUNX2 (Cell Signaling Technology, D1H7, 1:200) or TAZ (Cell Signaling Technology, E8E9G, 1:200) and α-SMA (Sigma-Aldrich A2547,1:500) overnight at 4°C. Slides were washed and incubated with appropriate secondary Alexa Fluor™ Plus 488–conjugated goat anti-mouse IgG (Invitrogen, 1:500) and Alexa Fluor 647–conjugated goat anti-rabbit IgG (Life technologies, 1:500), respectively, for 60 min. All sections were counterstained with nuclear DAPI (1:1,000) and stained slides were visualized by confocal microscope. For rat lung sections, 10-25 distal arterioles of 25-100 µm diameter were analyzed per rat.

For immunofluorescence staining of cultured cells, PASMC were seeded in 24-well plates prior to treatment. Cells were washed with cold PBS three times and fixed with 4% ice-cold paraformaldehyde (PFA) for 10 min at room temperature. After triple washing with PBS, cells were blocked with PBTB for 60 min. Cells were stained for RUNX2, TAZ, and α-SMA as described above, mounted with fluorescent mounting medium (Dako Cytomation), and imaged on an EVOS M5000 Imaging System (Thermo Fisher) or with confocal microscopy as described above.

2.5 Vascular calcification

For histochemical assessment of vascular calcification, 5 µm thick human PA or rat lung tissue sections were thawed and rehydrated as described above. Von Kossa staining was performed according to the manufacturer´s instructions (ab150687; Abcam, Cambridge, UK). In brief, silver nitrate solution was added, and slides were exposed to ultraviolet light for 60 min. After 2 rinses with distilled water, sodium thiosulfate solution was added, and slides were incubated for 2 min, and then washed twice with distilled water. Slides were incubated in Nuclear Fast Red solution for 5 min and then washed again twice with distilled water. Finally, slides were dehydrated with anhydrous ethanol and sealed with slide

mounting medium (DPX Mountant for histology, Sigma-Aldrich). Images were taken under a Zeiss microscope (Axioskop 40, Germany) and the calcified area (in black) was quantified as the percentage of the total imaged tissue area using Image J [34].

For alizarin red staining, human PA or rat lung tissue sections were stained with alizarin red solution (Sigma-Aldrich, TMS-008-C) for 5 min, images were acquired on a Zeiss microscope (Axioskop 40, Zeiss, Germany) in polarized light, and the calcified area (in red) was quantified as described above. For calcification in cultured human PASMC, cells were incubated for 72 hours with a calcification medium containing DMEM + 5% FBS, 50 µg/mL ascorbic acid, 2 mMol/L NaH_2PO_4, and 3mMol/L $CaCl_2$ as previously reported [15, 35]. Next, cells were rinsed with distilled water and stained with alizarin red solution for 5 min. After removal of the staining solution, cells were carefully rinsed with distilled water at least two times and imaged as described above.

For quantification of the respective free calcium content in snap-frozen human PA or rat lung samples, tissues were incubated overnight at 37°C in 0.6 Mol/L HCl. After centrifugation at 10,000 rpm for 5 min, calcium content in the supernatant was determined by use of the QuantiChrom Calcium assay kit (BioAssay Systems) according to the manufacturer's protocol. After washing with PBS, tissues were lysed with 0.1 Mol/L NaOH/0.1% SDS, total protein concentration was measured by Bradford assay (Bio-Rad Laboratories), and the calcium content was expressed relative to protein content.

2.6 RNA isolation and real-time quantitative polymerase chain reaction (RT-qPCR)

Total RNA was extracted from PAMSC by use of the RNeasy mini kit (#74104 Qiagen) according to the manufacturer´s protocol followed by RNA isolation. RNAs were reverse-transcribed into cDNA using the cDNA synthesis kit (#K1622, Thermo Fisher). RT-qPCR was performed on a CFX96 Real-time system (Fast SYBR Green Master Mix, #4385612, Thermo Fisher) with primers as listed in **Table 2**.

Table 2. Primer sequences used in real-time PCR for *GAPDH*, *RUNX2*, and *TAZ*

Gene	sequence (5′-3′)
GAPDH	Forward: GAAGGTGAAGGTCGGAGT
	Reverse: GAAGATGGTGATGGGATTTC
TAZ (WWTR1)	Forward: TTCCTAGGGTCTTGCCATGT

	Reverse: AGTCCTACGACGTGACCGAC
RUNX2	Forward: CTCCTACCTGAGCCAGATGA
	Reverse: CGGGGTGTAAGTAAAGGTGG

2.7 Western blotting

Human PA or rat lung tissue samples were ground in liquid nitrogen for protein extraction. Primary PASMC were lysed in radioimmunoprecipitation assay (RIPA) buffer with protease inhibitor complex (Roche, no.04693124001) and phosphatase inhibitors (Thermo Scientific, A32957). Samples were centrifuged (14,000g, 10 min, 4°C), and the protein concentration in the supernatant was determined by spectrophotometry (BCA Protein Assay Kit, 23227, Thermo Scientific). Samples were run on a sodium dodecyl sulfate-polyacrylamide gel (SDS-PAGE), followed by electrotransfer to a 0.45-µm pore size polyvinylidene fluoride (PVDF) membrane (Carl ROTH, Rolle). After blocking with 5% bovine serum albumin (BSA) in TBST buffer (Tris-buffered saline with 0.1% Tween-20), the following antibodies were applied overnight at 4°C.

Table 3. Primary antibodies for western blotting

Antibody	Manufacturer (Cat.No.)	Dilution
anti-RUNX2	Cell Signaling Technology, D1H7	1:1,000
anti-alkaline phosphatase	Abcam, ab65834	1:1,000
anti-osterix	Santa Cruz, sc-393325	1:500
anti-TGF-β	Abcam, ab179695	1:1,000
anti-TAZ	Cell Signaling Technology, E8E9G	1:1,000
anti-GAPDH	Cell Signaling Technology, 14C10	1:10,000
anti-β-actin	Abcam, Ab8226	1:1,000
anti-lamin B1	Proteintech, #12987-1-AP	1:5,000

Membranes were washed three times with TBST then incubated with HRP-conjugated secondary antibody (anti-mouse IgG, GE Healthcare, NA931-100UL, 1:5,000; anti-rabbit IgG, Abcam, ab97051, 1:5,000) for 1 hour at room temperature. Final detection of proteins was performed using the Clarity™ Western ECL substrate (Bio-Rad, 170-5060). For cell culture experiments, GAPDH or β-actin were used as housekeeping genes. In lung and

PA samples of PH-LHD rats and patients, respectively, these housekeeping genes are also frequently differentially regulated [28]; therefore, amido black staining was used as the loading control, and detected target proteins with molecular weights of 60 kDa (RUNX2), 57 kDa (ALP), or 45 kDa (osterix) were normalized to a lower molecular weight (~ 40 kDa) lane in amido black staining.

2.8 Extraction of nuclei from PASMC

Human PASMC were seeded in 100 mm dishes and grown to 80% confluence, followed by TGF-β treatment for 72 hours. Nuclear protein lysates were extracted by use of a Nuclear Extraction Kit (Abcam, ab113474) according to the manufacturer's instructions. Fractionated samples were analyzed by western blotting using anti-RUNX2, anti-TAZ, and anti-lamin B1 antibodies as described above.

2.9 Cycloheximide chase assay and proteasome inhibition

Human PASMC were seeded on 6-well plates and grown to 80-90% confluence, followed by TGF-β treatment for 72 hours. After 66 hours, PASMC were treated with the YAP/TAZ inhibitor Verteporfin, the protein synthesis inhibitor cycloheximide (CHX) and/or the proteasome inhibitor MG132 for 6 hours. Protein samples were collected and analyzed by immunoblotting as described above.

2.10 Co-immunoprecipitation

Human PASMC were treated with TGF-β (10 ng/mL for 72 hours) or vehicle and Verteporfin (1 mMol/L) or vehicle were added for the last 6 hours. To reduce non-specific binding to the beads during immunoprecipitation, cell lysates were pre-cleared by incubation with pre-washed Protein G magnetic beads (Dynabeads™, Thermo Fisher) in a ratio of 1,000:20 at 4°C overnight. After magnetic beads were separated from lysates by a magnetic separation rack, the pre-cleaned lysates were transferred to clean tubes and antibodies directed against RUNX2 (Cell signaling Technology, D1H7, 1:1000) or ubiquitin (Proteintech, 10201-2-AP, 1:1000) were added, followed by overnight incubation at 4°C. To collect the formed complex composed of anti-RUNX2 antibodies bound to RUNX2 and possible RUNX2-binding partners or anti-ubiquitin antibodies bound to ubiquitinated proteins including RUNX2, respectively, protein G beads were added the next

day for 3 hours at 4°C. After washing the beads 5 times, the supernatant was carefully removed and 3x concentrated SDS-PAGE sample loading buffer with DDT was added to the pellet. Samples were boiled at 95°C for 10 min and the immunoprecipitated pellet as well as the original input (cell lysate) as corresponding control were immunoblotted for RUNX2, TAZ, and ubiquitin (Proteintech,10201-2-AP, 1:2000) protein levels as described above. Anti-light chain-specific antibody for western blotting after IP was used as a secondary antibody (Jackson ImmunoResearch, Peroxidase IgG Fraction Monoclonal Mouse Anti-Rabbit IgG, light chain specific, 211-032-171).

2.11 Statistical analysis

Statistical analyses were performed using GraphPad Prism software (GraphPad Prism 8.0; GraphPad Software Inc., La Jolla, CA). All data are presented as bar graphs with individual data points, with bars showing means ± SEMs. Normal distribution and equality of variance were assessed by Shapiro-Wilk test and Brown-Forsythe test (modified Levene test), respectively. For parametric and non-parametric data, respectively, the Student's t-test (two-tailed) or Mann-Whitney test were used to compare two groups. For > 2 groups, one-way analysis of variance (ANOVA) was applied with Tukey's post-hoc test. P-values<0.05 were considered as statistically significant.

3. Results

3.1 RNA sequencing of pulmonary artery (PA) in PH-LHD rats and patients

Previously, the Kuebler lab successfully established a preclinical model of PH-LHD in rats following subcoronary aortic banding (AoB). Data obtained by Dr. Mariya Kucherenko and Pengchao Sang in the Kuebler and Knosalla lab of the Charité, and kindly provided for use in this thesis, show that AoB not only leads to an increase in left ventricular systolic pressure (LVSP) and left ventricular hypertrophy (assessed as weight of the left ventricle plus the septum relative to body weight), but also to a significant elevation in right ventricular systolic pressure (RVSP) and right ventricular hypertrophy (determined as right ventricular weight relative to body weight) as a characteristic feature of PH-LHD that can be detected as early as 3 weeks (3w) post-surgery [31, 36], and is prominent at 5 weeks (5w) and 9 weeks (9w) post-surgery (**Fig. 2**). Corresponding sham-operated animals served as controls.

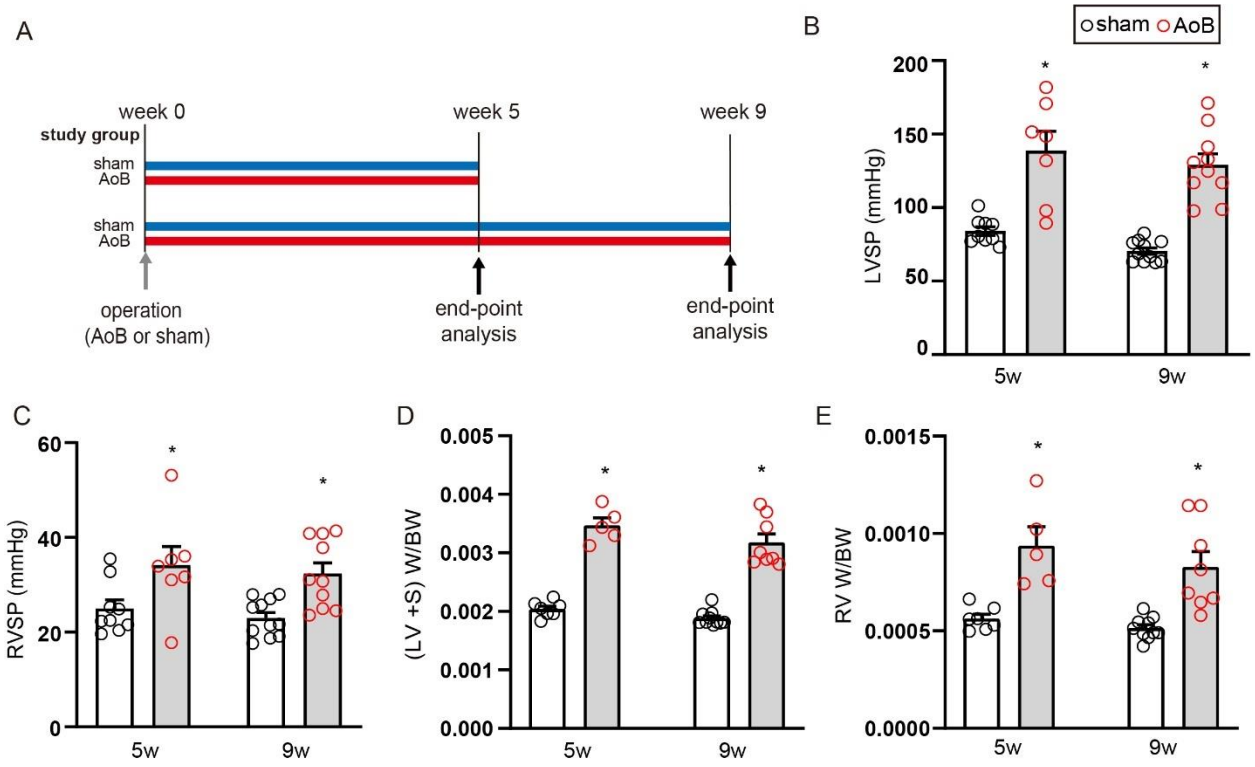

Figure 2. Cardiac hemodynamics and biventricular hypertrophy in PH-LHD rats.

A) Experimental protocol for hemodynamic characterization of rats with aortic banding (AoB)-induced PH-LHD, as well as sham-operated controls, at 5 weeks (5w) and 9 weeks (9w) post-surgery. Quantitative data show (**B**) left (LVSP) and (**C**) right ventricular systolic pressure (RVSP), as determined by cardiac catheterization, and (**D**) left and (**E**) right ventricular hypertrophy, assessed as the weight of the left ventricle plus septum (L V+S) or the right ventricle (RV) relative to body weight (BW), respectively (n=5–11 rats per group,

*p<0.05 versus sham at corresponding time point). Data kindly provided for use in this thesis by Dr. Mariya Kucherenko and Pengchao Sang.

To probe for potential mechanisms of PA remodelling in PH-LHD, Dr. Mariya Kucherenko of the Kuebler and Knosalla lab at the Charité previously performed genome-wide transcriptomic analyses of tissue samples from the main PA obtained from AoB and sham rats at 5 weeks and 9 weeks post-surgery. Using gene ontology (GO) term analysis, these analyses identified enrichment in differentially expressed genes associated with the GO terms "ossification" (GO:0001503) and "osteoblast differentiation" (GO:0001649). RUNX2, a key transcription factor involved in osteogenesis and vascular calcification, was enriched at 5 weeks post-surgery along with a substantial number of genes within the GO term "ossification", while differential expression was less pronounced in the more chronic stage at 9 weeks post-surgery, although RUNX2 was still upregulated (**Fig. 3A**). At the protein interaction network level, Markov clustering analysis revealed a central regulatory role for RUNX2 in the network of differentially regulated genes (**Fig. 3B**).
Analogous genome-wide transcriptomic analyses on human pulmonary trunk tissue samples obtained from patients with PH-LHD and healthy heart donors during heart transplantation in collaboration with Prof. Dr. C. Knosalla (DHZC) similarly revealed a significant dysregulation of genes associated with ossification and osteoblast differentiation, including RUNX2, in PA of PH-LHD patients compared to healthy-heart donors (**Fig. 3C**). Specifically, significant differential regulation (p<0.05) of a total of 50 genes associated with the gene ontology terms "ossification" (GO:0001503) and "osteoblast differentiation" (GO:0001649) was identified in patients with PH-LHD compared to healthy-heart donors (**Fig. 3C**).

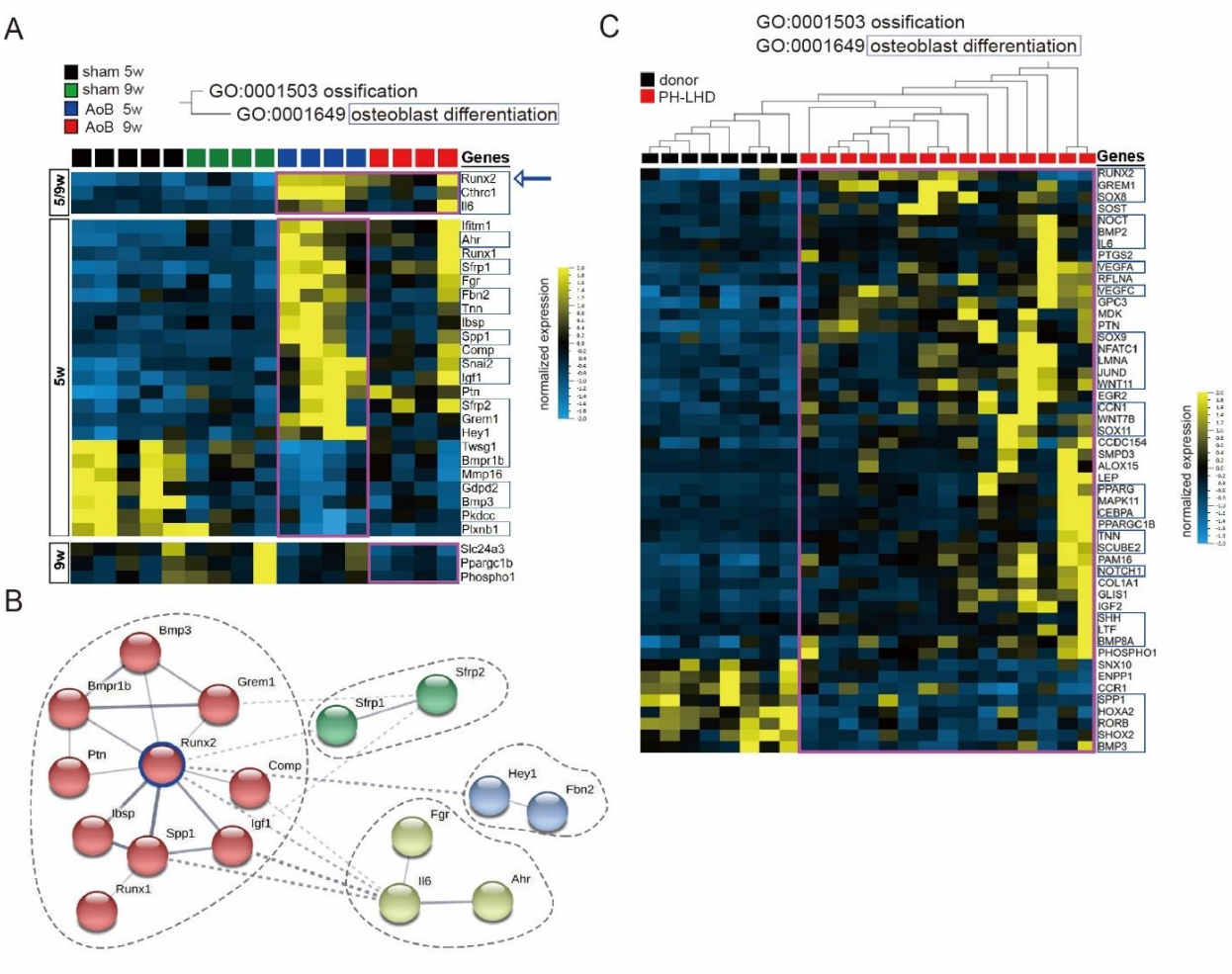

Figure 3. Differential gene regulation in PA of AoB rats and human PH-LHD patients, respectively, relative to corresponding controls.

A) Heat map depicts differentially expressed genes (p<0.05) associated with the gene ontology (GO) terms "ossification" (GO:0001503) and "osteoblast differentiation" (GO:0001649) in PA of rats subjected to either supracoronary aortic banding (AoB) surgery or sham operation at 5 or 9 weeks post-surgery, respectively (n=4-5 each). Vertical arrangement of the genes indicates their differential regulation between the AoB and sham groups at both 5 and 9 weeks (top; 5/9w), followed by genes significantly dysregulated at either only 5 weeks (center; 5w) or 9 weeks (bottom; 9w). **B**) Protein interaction network analysis, combined with Markov clustering, reveals the osteogenic transcription factor RUNX2 as a central regulator of differential gene expression in PA of AoB rats. **C**) Heat map illustrates differentially expressed genes (p<0.05) within the GO terms "ossification" (GO:0001503) and "osteoblast differentiation" (GO:0001649) in PA of PH-LHD patients (n=15) versus those of healthy-heart donors (n=8). Data kindly provided for use in this thesis by Dr. Mariya Kucherenko.

3.2 Vascular calcification of pulmonary artery (PA) in a rat model of pulmonary hypertension due to left heart disease (PH-LHD)

Based on the prior findings from bulk RNA sequencing, which indicated the presence of osteogenic and ossification processes in the PA of PH-LHD rats, I started my project by performing histochemical analyses to probe directly for vascular calcification in the PA of AoB rats. Indeed, von Kossa staining revealed a significant increase in calcification in both the proximal and distal PAs of AoB rats at 5w and 9w post-surgery compared to sham animals (**Fig. 4A-C**). Similarly, alizarin red staining identified calcium deposits in the proximal and distal PAs at 9w, yet not at 5w post-surgery (**Fig. 4D-F**).

The presence of vascular calcification in AoB rats was further validated by a colorimetric assessment of calcium content in lung tissue, which showed increased calcium deposition at 5w post-surgery in AoB rats, with a similar trend at 9w post-surgery compared to sham animals which, however, failed to reach statistical significance (p=0.0597) (**Fig. 4G**).

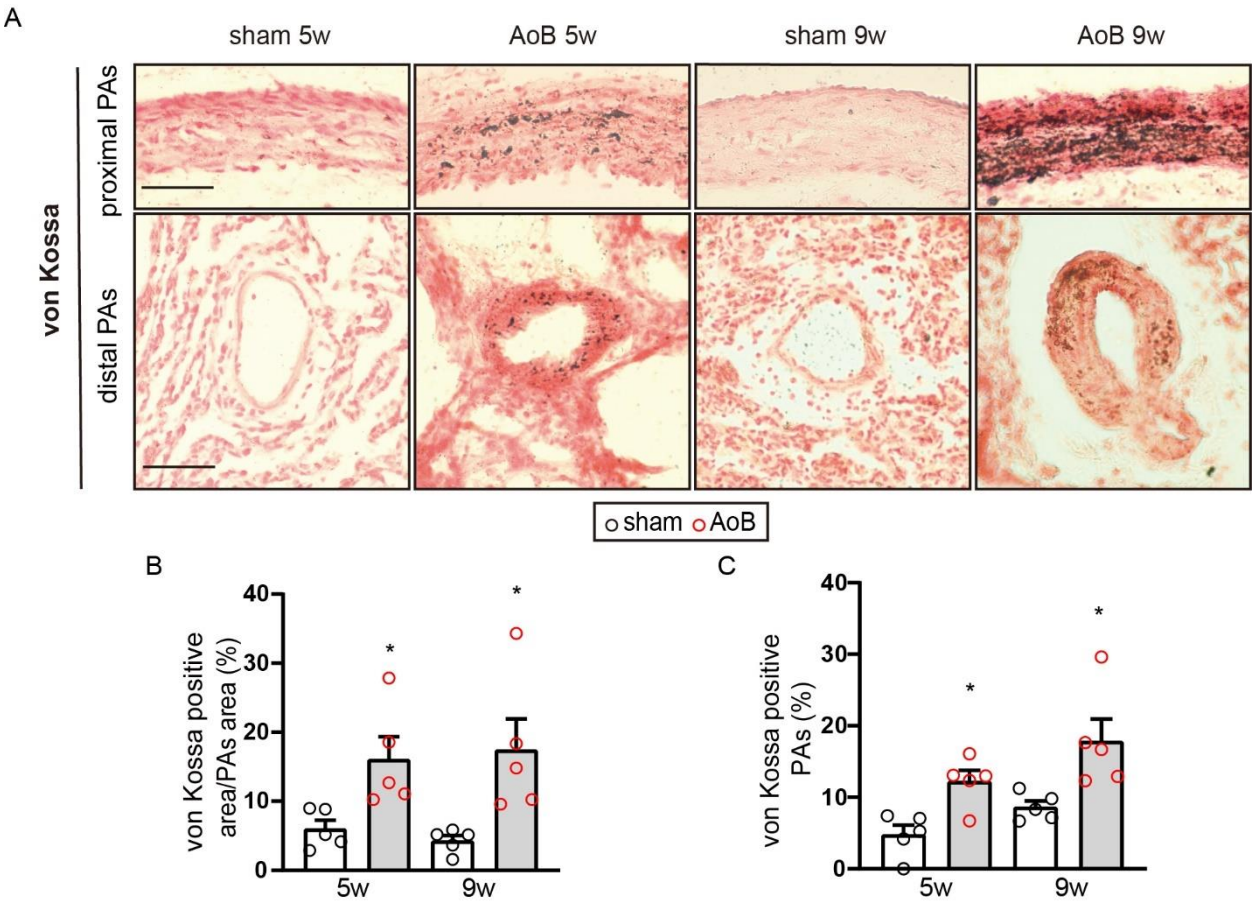

Figure 4 (continues on next page)

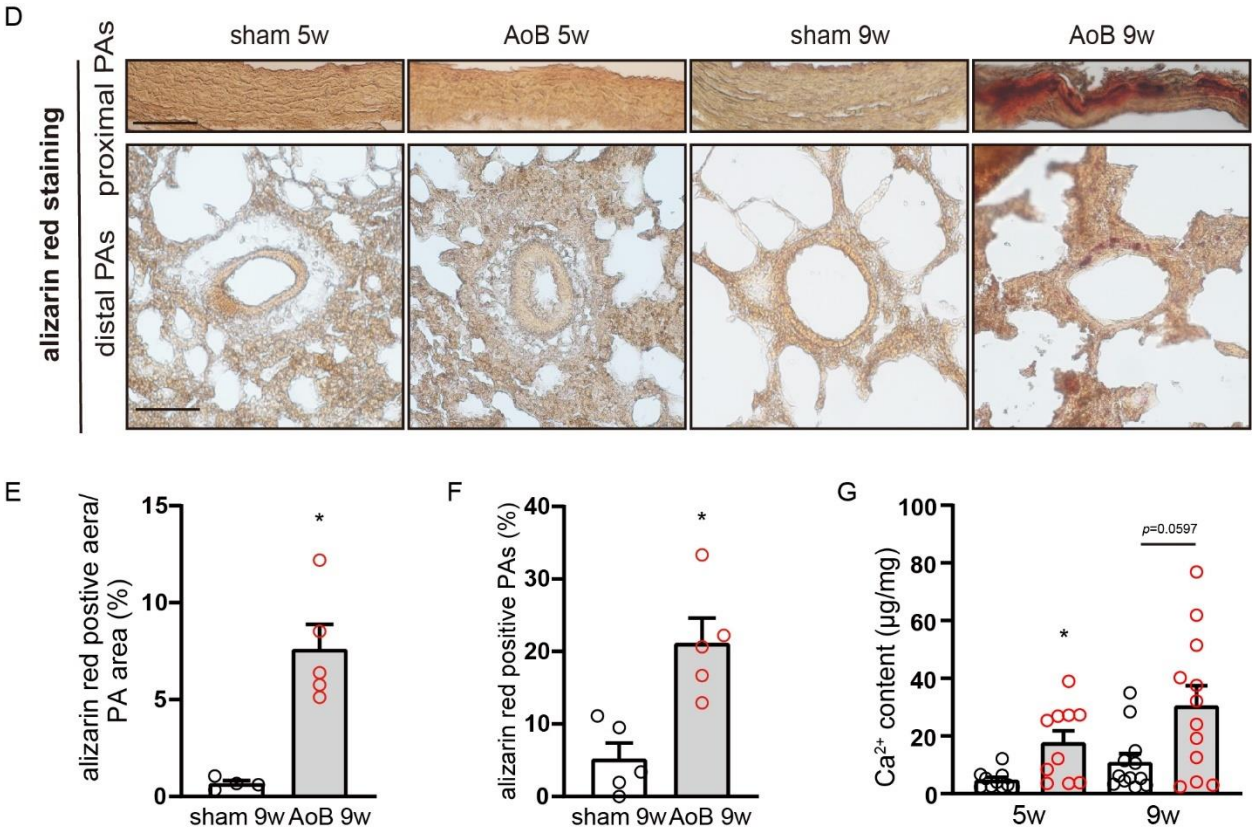

Figure 4. Pulmonary artery calcification in PH-LHD rats.

A) Representative images of von Kossa stained histological sections indicate marked calcification in the proximal (top, scale bar: 50 µm) and distal (bottom, scale bar: 50 µm) pulmonary arteries (PAs) of AoB rats. (**B**) Quantitative analysis of the fraction of von Kossa-positive vessel wall area in proximal PAs, and (**C**) the fraction of von Kossa-positive vessels in distal PAs (n=5 per group). **D-F**) Representative images of alizarin red stained histological sections of proximal (upper panel, scale bar: 100 µm) and distal (lower panel, scale bar: 50 µm) PAs show calcium deposits in AoB rats 9 weeks post-surgery. Bar graph and scatter plots show (**E**) the fraction of alizarin red-positive vessel wall area in proximal PAs, and (**F**) the percentage of alizarin red-positive vessels in distal PAs (n=4-5 per group, **p*<0.05 versus sham). Please note that due to the absence of alizarin-red positive staining at 5 weeks post-surgery, quantitative data are only shown for the time point of 9 weeks. **G**) Bar graph and scatter plots depict calcium content in lung tissue of AoB and sham rats at 5 and 9 weeks post-surgery (n=10-12 per group). **p*<0.05 versus sham at the corresponding time point.

3.3 Vascular calcification of PA in PH-LHD patients

To similarly investigate the presence of PA calcification in patients with PH-LHD, we next performed von Kossa and alizarin red staining on PA sections obtained from patients with clinical PH-LHD as defined in Section 2.1. Von Kossa staining (**Fig. 5A, B**) and alizarin red staining (**Fig. 5C, D**) revealed the presence of calcium-rich biomineralization and calcification in the proximal PA of PH-LHD patients, yet calcification was absent in the PA of

healthy-heart donors. Quantification of calcium content confirmed a significant increase in PA of PH-LHD patients compared to healthy-heart donors (**Fig. 5E**).

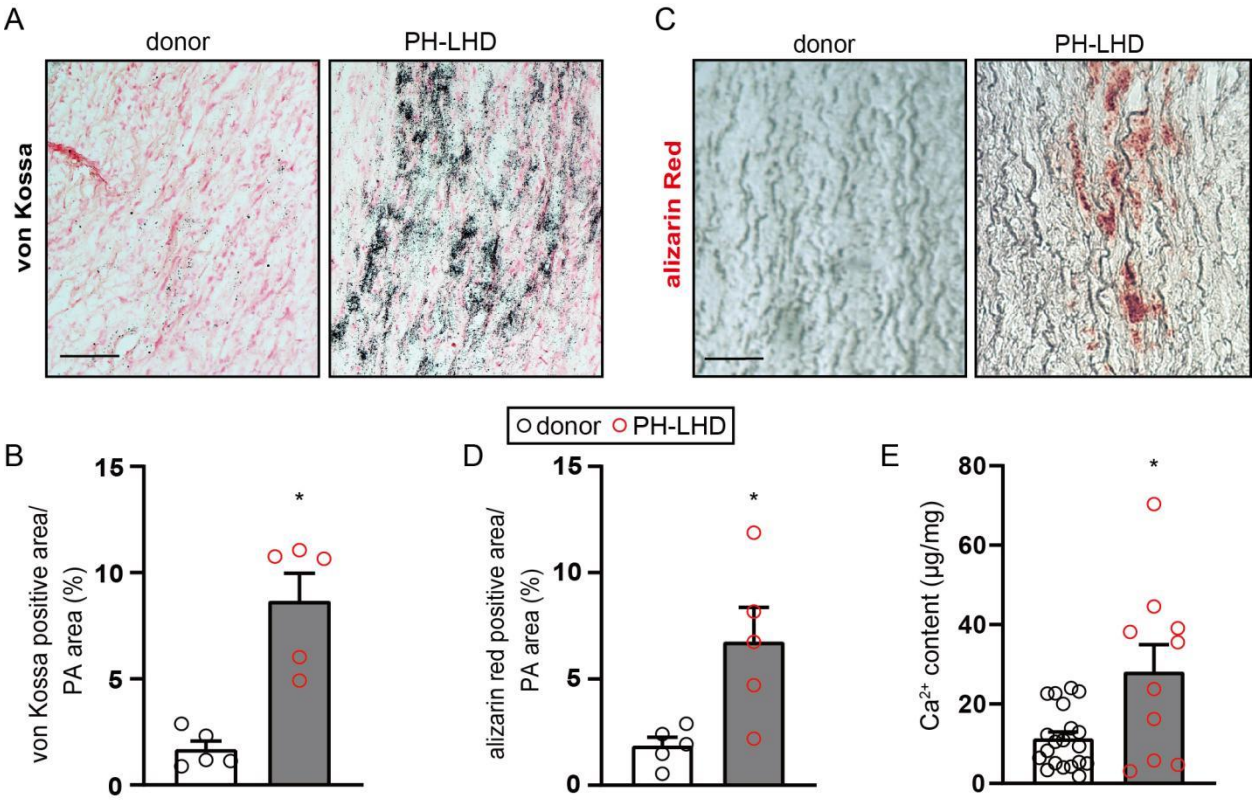

Figure 5. Pulmonary artery calcification in PH-LHD patients.

A) Representative images and quantitative analysis (**B**) of von Kossa stained sections (scale bar: 100 µm) show vascular calcification in PA of PH-LHD patients relative to healthy-heart donors (n=5 each group). Representative images (**C**) of alizarin red stained sections (scale bar: 100 µm) and quantitative analysis (**D**) corroborate this finding. **E**) Bar graph and scatter plot show calcium content in PA samples of healthy-heart donors (n=20) and PH-LHD patients (n=10), respectively. *p<0.05 versus healthy-heart donors.

Consequently, PA calcification is equally prevalent in the clinical setting of PH-LHD patients and in a preclinical rat model of PH-LHD. This finding highlights the clinical significance of PA calcification and underscores the translational relevance of the rat AoB model.

3.4 RUNX2 upregulation and nuclear localization in preclinical and clinical PH-LHD

3.4.1 RUNX2 upregulation and nuclear localization in PA of AoB rats

Based on the established role of RUNX2 as a master regulator in osteogenesis and vascular calcification, and its central involvement in the network of differentially regulated genes in our transcriptomic datasets, we specifically investigated the protein expression

of RUNX2 and its nuclear translocation (as indicator of its activation) in preclinical and clinical PH-LHD. In lungs of AoB rats, immunoblotting showed an upregulation of RUNX2, along with the RUNX2-regulated osteogenic markers alkaline phosphatase (ALP) and osterix relative to sham controls (**Fig. 6A**). Immunofluorescence staining further revealed an increased nuclear abundance of RUNX2 in the distal PA of lung tissue sections from AoB rats compared to sham rats (**Fig. 6B**).

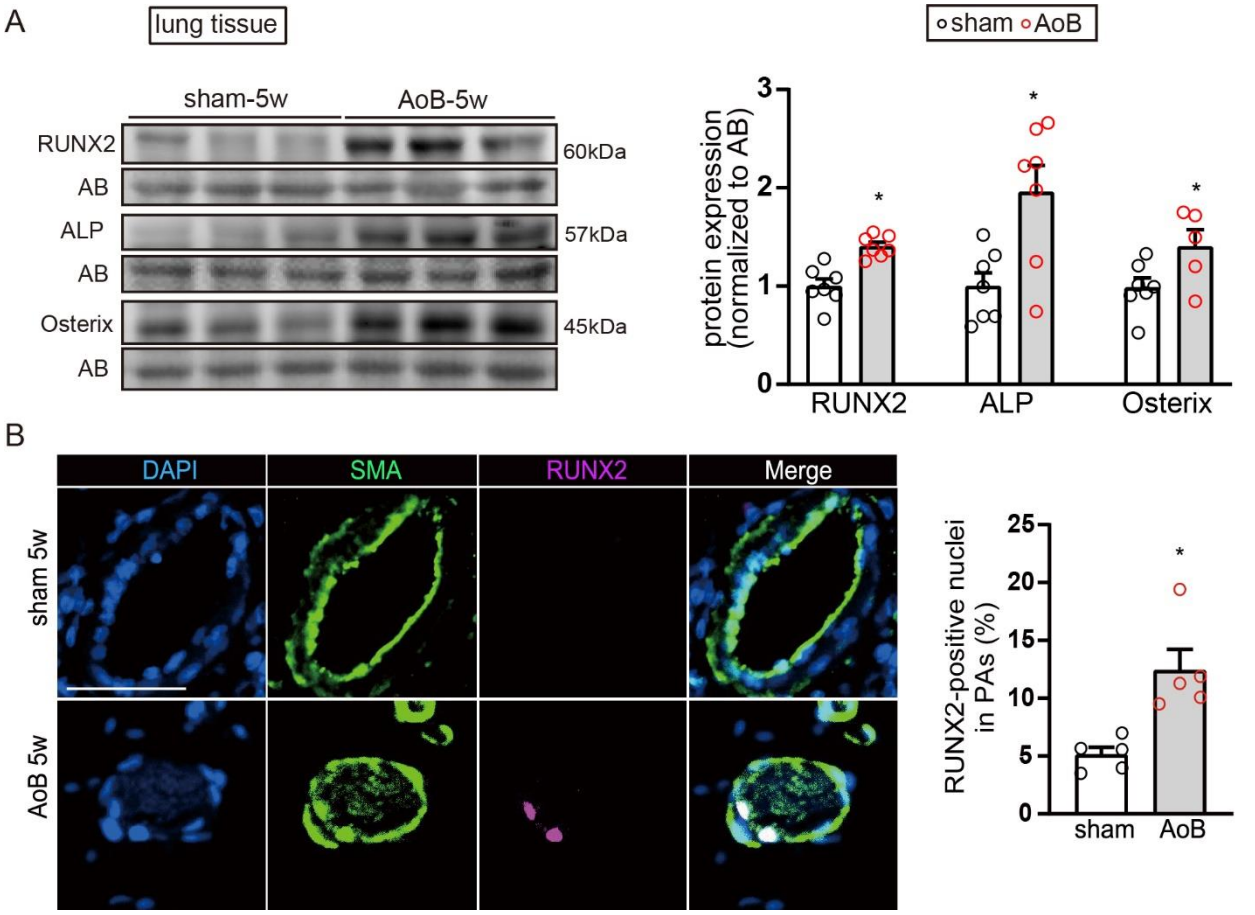

Figure 6. RUNX2 is upregulated in lung tissue and localizes to the nucleus in PA of PH-LHD rats.
A) Representative western blots and corresponding densitometric quantification (n=5-7 per group) show increased expression of RUNX2, alkaline phosphatase (ALP) and osterix in lung tissue of AoB rats relative to sham controls (**p*<0.05 vs. sham). **B**) Representative z-stack fluorescence microscopic images of lung tissue immunostained for RUNX2 (purple) and for α-SMA (green), and counterstained with DAPI (blue), and the corresponding quantification of RUNX2 positive nuclei in SMA-positive cells of the vascular wall show increased nuclear abundance of RUNX2 in distal PA of AoB rats relative to sham controls (n=5 per group; scale bar: 50 µm, **p*<0.05 versus sham). AB: amido black.

3.4.2 RUNX2 upregulation and nuclear localization in PA and PASMC of PH-LHD patients

Analogously, we detected an upregulated expression of RUNX2, ALP, and osterix in PA of patients with PH-LHD compared to healthy-heart donors (**Fig. 7A**). To specifically investigate whether PASMC derived from PH-LHD patients undergo phenotypic transformation towards an osteogenic-like phenotype, we further probed for the expression and activation of RUNX2 in primary PASMC isolated from the patients' PA. Consistent with our findings in rat lung tissue and human PA, PASMC obtained from PH-LHD patients expressed increased protein levels of RUNX2, ALP, and osterix (**Fig. 7B**).

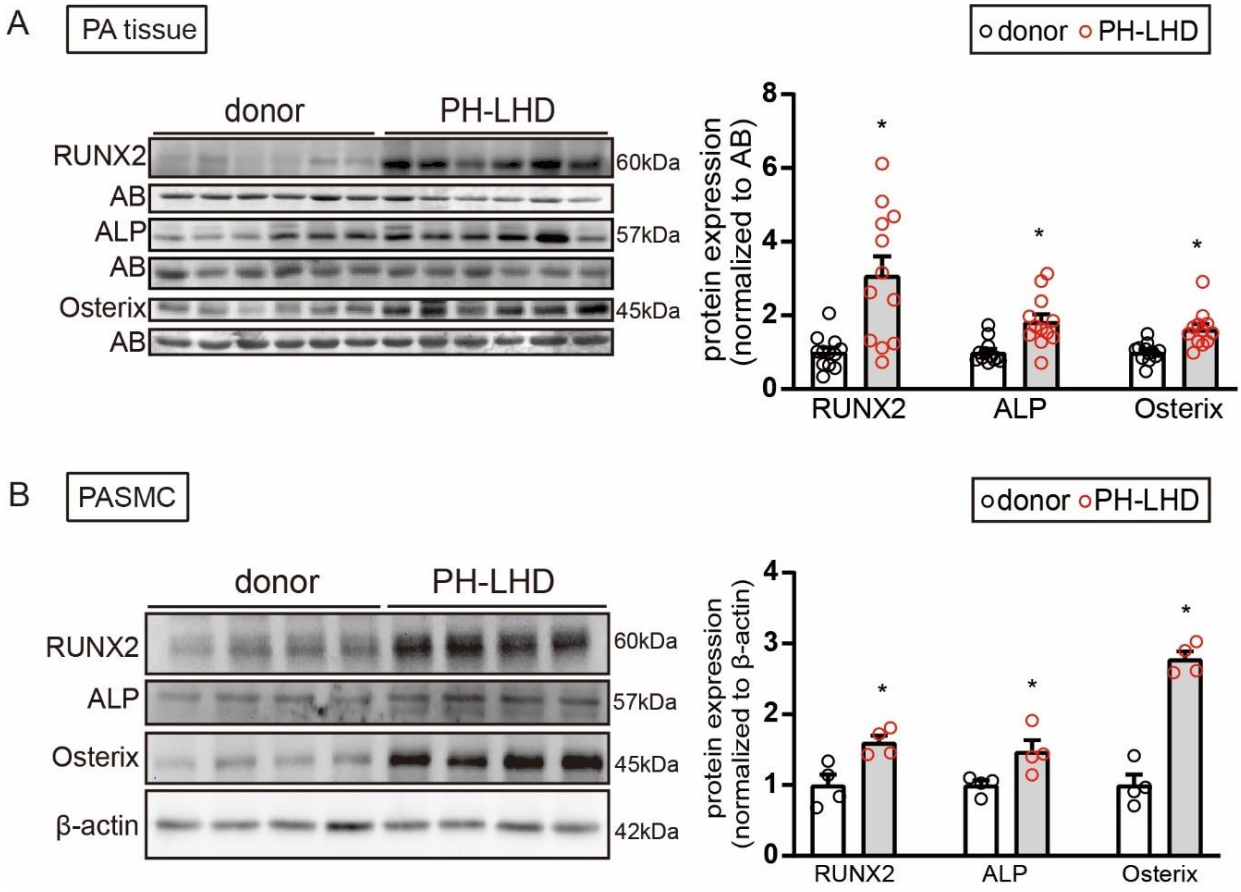

Figure 7. RUNX2 is upregulated in PA and PASMC of PH-LHD patients.

A) Representative western blots and corresponding densitometric quantification (n=12 per group) show increased expression of RUNX2, ALP, and osterix in PA of PH-LHD patients versus those of healthy-heart donors (**p*<0.05 versus donor). **B**) Representative western blots and corresponding densitometric quantification (n=4 per group) show increased expression of RUNX2, ALP, and osterix in PASMC isolated from PA of PH-LHD patients compared to those from healthy-heart donors (**p*<0.05 versus donor). AB: amido black.

Immunostained PA sections demonstrated a marked increase in the nuclear localization of RUNX2 (**Fig. 8A**), indicating enhanced expression and nuclear translocation of RUNX2.

This observation was further supported by immunofluorescence staining of PASMC from PH-LHD patients, again showing increased nuclear abundance of RUNX2 compared to PASMC from healthy-heart donors (**Fig. 8B**).

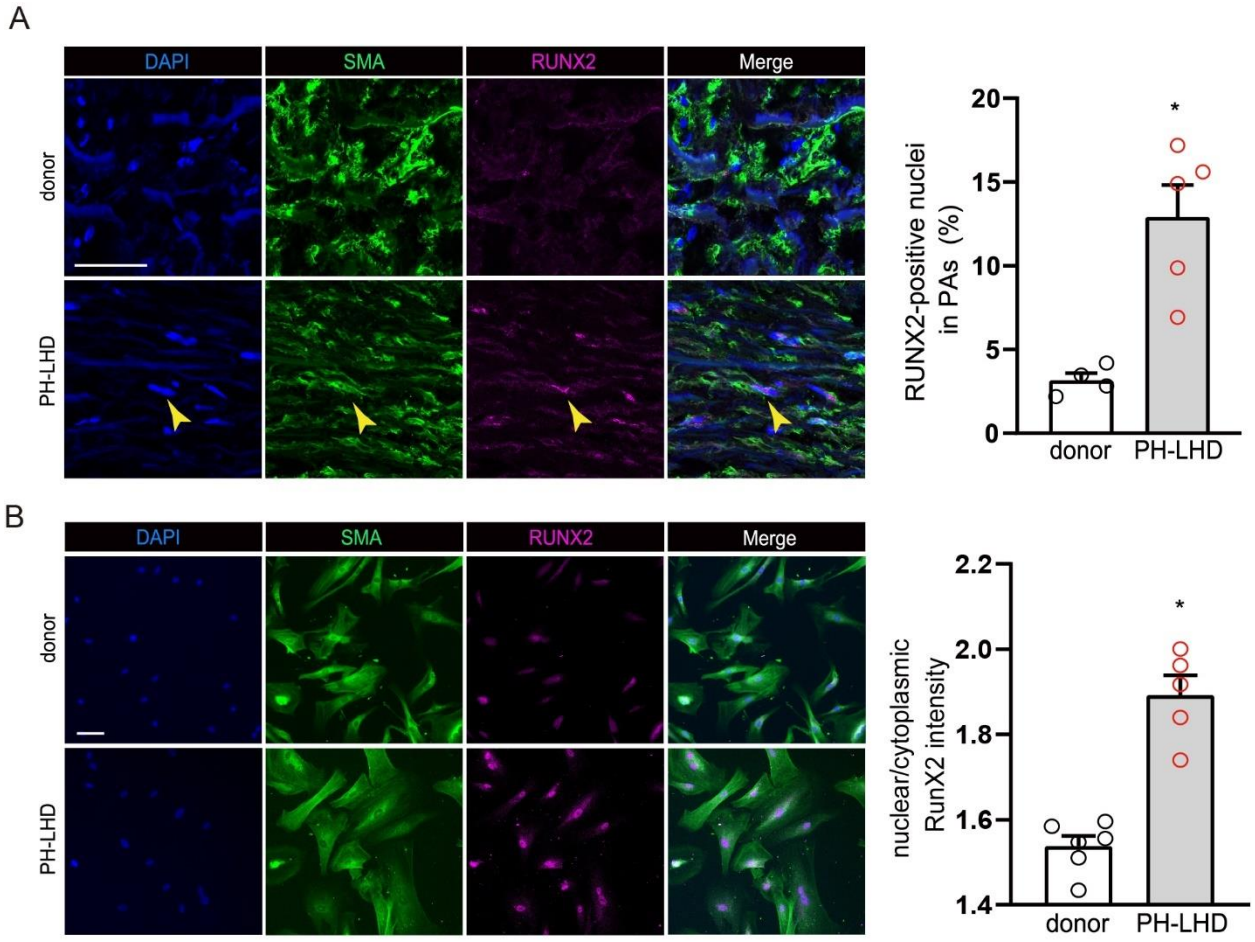

Figure 8. RUNX2 localizes to the nucleus in PA and PASMC of PH-LHD patients.

A) Representative single z-plane fluorescence microscopic images of PA immunostained for RUNX2 (purple) and α-SMA (green), and counterstained with DAPI (blue), and the corresponding quantification of RUNX2 positive nuclei in SMA-positive cells show increased expression and nuclear translocation of RUNX2 in PA of PH-LHD patients relative to those of healthy-heart donors (n=4-5 per group, scale bar: 50 µm, **p*<0.05 versus donor). **B**) Representative fluorescence microscopic images of isolated PASMC immunostained for RUNX2 (purple) and α-SMA (green), and counterstained with DAPI (blue), and the corresponding quantification of the nuclear-to-cytoplasmic ratio of RUNX2 fluorescence intensity show increased expression and nuclear translocation of RUNX2 in PASMC isolated from PA of PH-LHD patients as compared to those from PA of healthy-heart donors (n=5-6 per group, scale bar: 100 µm, **p*<0.05 versus donor).

To further consolidate the emerging osteogenic transdifferentiation of PASMC in PHLHD, we next tested whether PASMC from PH-LHD patients exhibit an increased propensity

for calcification compared to control PASMC. When cultured in a mineral-enriched calcification medium, PASMC from PH-LHD patients displayed a higher rate of calcification compared to PASMC from healthy-heart donors (**Fig. 9A**).

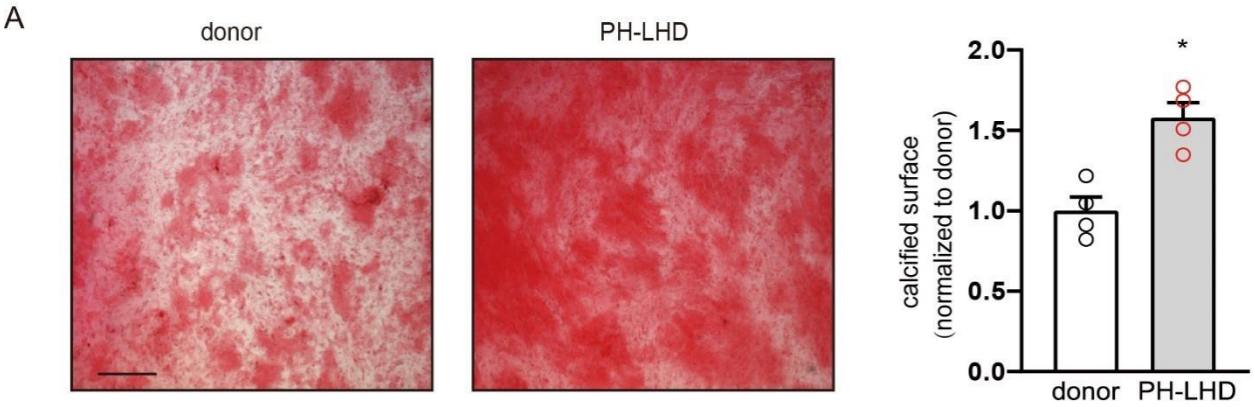

Figure 9. PASMC from PH-LHD patients show an increased propensity for calcification *in vitro* relative to healthy-heart donors.

A) Representative images show calcification (alizarin red staining) in PASMC isolated from PA of PH-LHD patients or healthy-heart donors over 72 hours culture in calcification medium. The corresponding quantification shows calcified area as percent of total surface area, normalized to healthy-heart donors (n=4 per group, scale bar: 100 µm, *p<0.05 versus donor).

Collectively, these findings show upregulation and nuclear translocation of RUNX2, which is associated with an osteogenic transdifferentiation of PASMC in PH-LHD.

3.5 Transforming growth factor-β (TGF-β) is increased in preclinical and clinical PH-LHD and replicates the PH-LHD phenotype of PASMC *in vitro*

3.5.1 TGF-β is increased in PH-LHD patients and AoB rats

To investigate the molecular mechanisms that regulate the expression of RUNX2 in PH-LHD, we aimed to replicate our findings in PASMC derived from patients with PH-LHD in a relevant *in vitro* scenario. Given its demonstrated role in lung vascular remodeling [33] and its reported ability to induce RUNX2 in pluripotent mesenchymal or osteoblastic cells [37, 38], we considered TGF-β as a potential candidate stimulus for the osteogenic transdifferentiation of PASMC in PH-LHD.

Western blot analysis revealed increased circulating levels of both monomeric and mature TGF-β in plasma of PH-LHD patients as compared to healthy controls (**Fig. 10A,A'**). Increased levels of mature TGF-β were similarly detected in plasma of AoB rats (**Fig.**

10B,B'), and latent TGF-β levels were elevated in AoB lungs as compared to sham controls (**Fig. 10C,C'**).

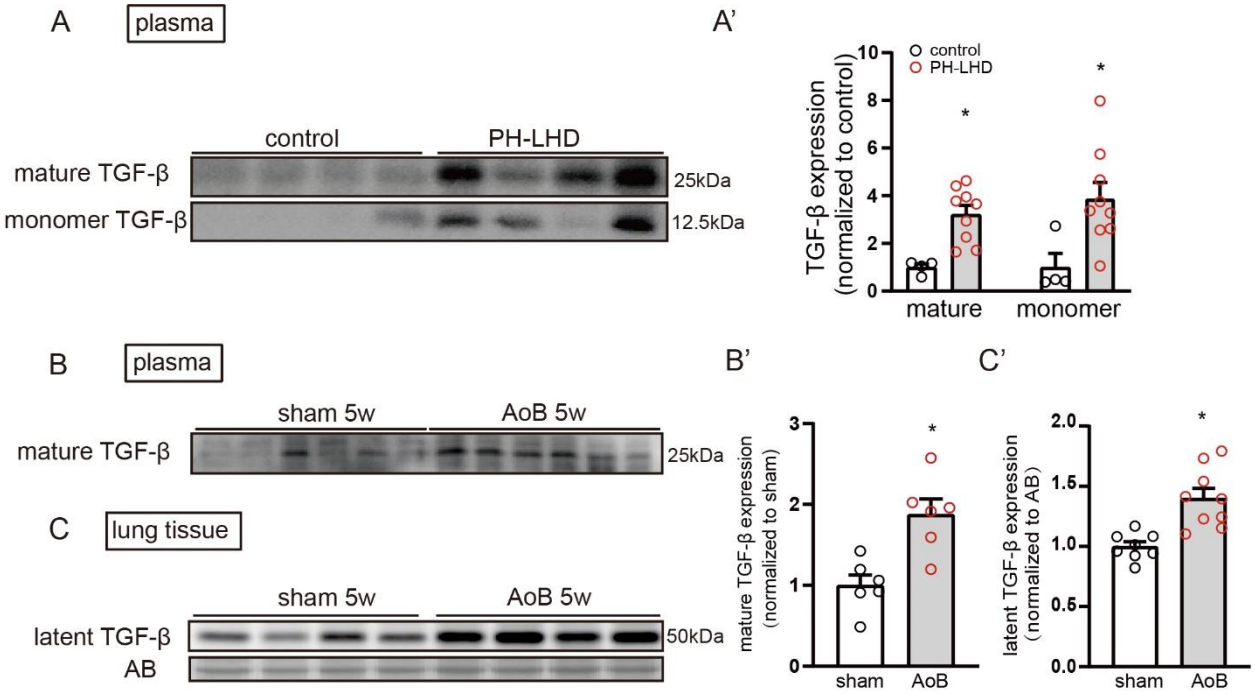

Figure 10. TGF-β is increased in plasma of PH-LHD patients and in plasma and lung tissue of AoB rats.

A) Representative western blots and (**A'**) corresponding densitometric quantification (n=4-9 per group) show increased protein levels of both monomeric and mature TGF-β in plasma of PH-LHD patients as compared to controls from three males aged 44, 54, and 39 years, and one 36-year-old female (*p<0.05 versus control). **B**) Representative western blots and (**B'**) corresponding densitometric quantification show increased levels of mature TGF-β in the plasma of AoB rats 5 weeks post-surgery as compared to corresponding sham controls (n=6 each group, *p <0.05). **C**) Representative western blots and (**C'**) corresponding densitometric quantification show increased levels of latent TGF-β in lung tissue of AoB rats 5 weeks post-surgery as compared to corresponding sham controls (n=8-9 each group, *p <0.05 versus sham).

3.5.2 TGF-β stimulation of PASMC replicates osteogenic transformation *in vitro*

Next, we tested whether increased TGF-β levels could replicate the osteogenic transdifferentiated phenotype of PASMC previously identified by us in clinical and preclinical PH-LHD. Stimulation of PASMC with TGF-β resulted in a progressive upregulation of RUNX2 mRNA expression (**Fig. 11A**) and an increase in RUNX2 protein levels at 72 hours (**Fig. 11B,B'**). Consistent with the activation and nuclear translocation of the transcription factor by TGF-β, RUNX2 protein was specifically enriched in isolated nuclear extracts from PASMC (**Fig. 11C,C'**).

Immunofluorescence staining further supported the latter finding by detecting increased nuclear abundance of RUNX2 in TGF-β-stimulated PASMC (**Fig. 11D,D'**). Finally, when cultured in calcification medium, TGF-β-stimulated PASMC exhibited an enhanced propensity for calcification (**Fig. 11E,E'**).

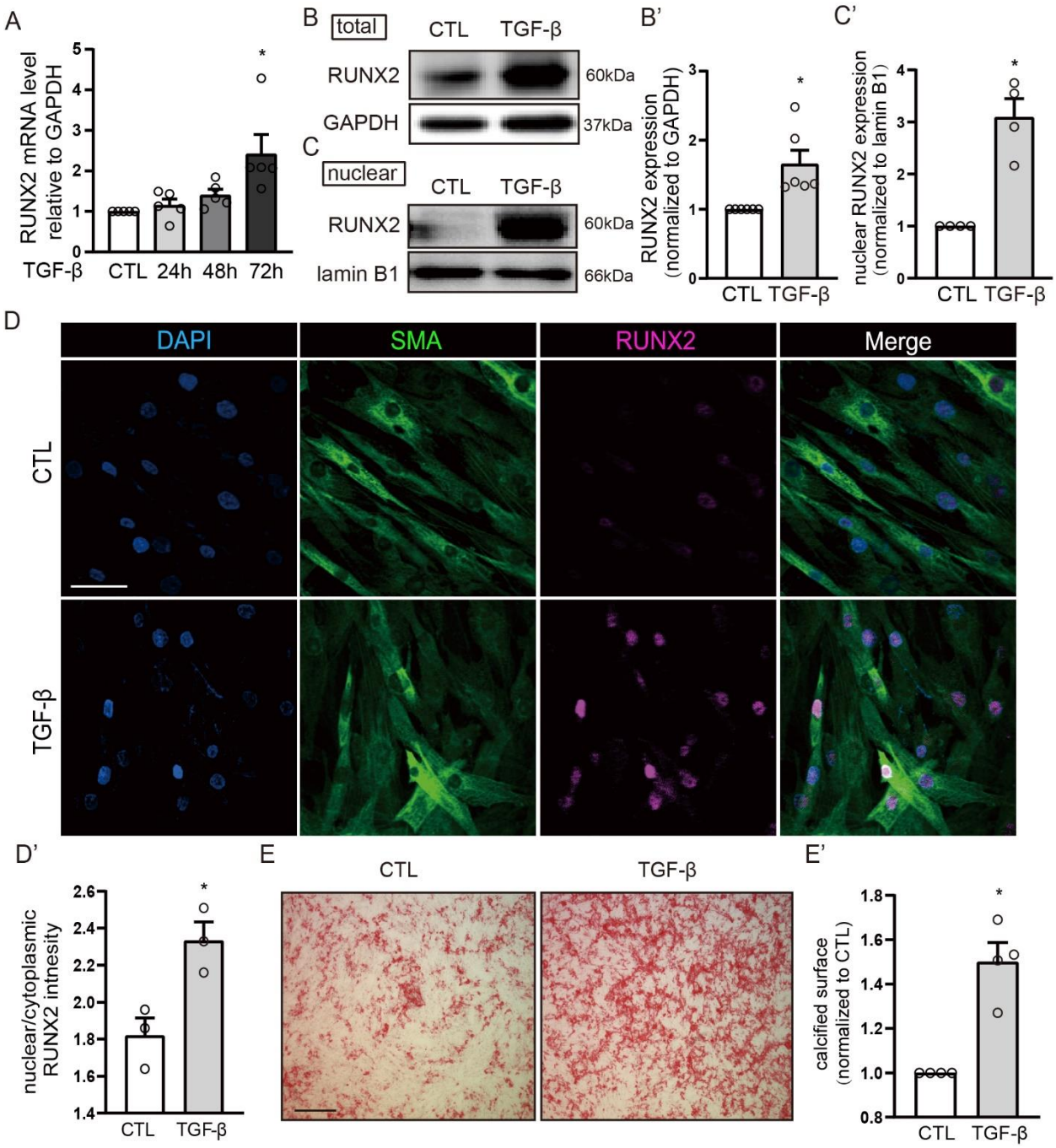

Figure 11. TGF-β stimulation of PASMC replicates osteogenic transformation *in vitro.*

A) mRNA expression levels as determined by real-time PCR show a time-dependent increase in RUNX2 expression in PASMC following stimulation with 10 ng/mL TGF-β or vehicle control (CTL) (n=5 biological replicates per group, **p*<0.05 versus CTL). **B,C**) Representative western blots and (**B',C'**) corresponding densitometric quantification show RUNX2 protein expression in TGF-β (10 ng/mL for 72 hours) stimulated

PASMC (**B** and **B'**; n=6 per group) and their isolated nuclear extracts (**C** and **C'**; n=4 per group) as compared to vehicle treated controls (*p<0.05 versus CTL). **D**) Representative fluorescence microscopic images of PASMC immunostained for RUNX2 (purple) and α-SMA (green), and counterstained with DAPI (blue), and the (**D'**) corresponding quantification of the nuclear-to-cytoplasmic ratio of RUNX2 fluorescence intensity show increased nuclear abundance of RUNX2 upon treatment with TGF-β (10 ng/mL for 72 hours) relative to controls (n=3 per group, scale bar: 50 µm, *p<0.05 versus CTL). **E**) Representative images show calcification (alizarin red staining) in PASMC treated with TGF-β (10 ng/mL) or vehicle for 72 hours in calcification medium. **E'**) Corresponding quantification shows calcified area relative to controls (n=4 per group, scale bar: 100 µm, *p<0.05 versus CTL).

Here, we show that levels of TGF-β are equally elevated in plasma of both humans and rats with PH-LHD, as well as in rat PH-LHD lungs. Treatment with TGF-β effectively replicated the characteristics of the osteogenic PASMC phenotype detected in PH-LHD patients and rats *in vitro*. These data indicate TGF-β as a candidate mechanism that may contribute to PA calcification *in vivo*, and may be utilized as an *in vitro* surrogate stimulus to dissect the cellular mechanisms of PASMC osteogenic transdifferentiation.

3.6 TAZ upregulation and nuclear localization

3.6.1 TAZ expression and activation is increased in PASMC of PH-LHD patients and AoB rats

In terms of the molecular mechanism underlying the increase in RUNX2 abundance and nuclear translocation induced by TGF-β treatment *in vitro* and detected in PH-LHD *in vivo*, we considered a potential involvement of the transcriptional co-activator TAZ, a critical constituent of the HIPPO signaling pathway, based on the rationale that: i) TAZ signaling is induced by TGF-β in mesenchymal and kidney tubular cells [21] as well as by mechanical stress [21]; ii) activation of TAZ (and/or YAP) contributes to lung vascular remodeling in PH [17, 39]; and iii) TAZ synergistically interacts with RUNX2, forming a master transcription factor complex that drives osteoblastogenesis [20].
Therefore, increased TAZ signaling, either through elevated TAZ expression or enhanced nuclear translocation, emerges as a potential pathway that may trigger or enhance RUNX2-mediated osteogenic calcification in response to mechanical stress and/or TGF-β, i.e. the biochemical and biomechanical context characteristic of PH-LHD.

By immunoblotting, we detected significant upregulation of TAZ in PA (**Fig. 12A,A'**) and PASMC (**Fig. 12B,B'**) of PH-LHD patients as compared to healthy-heart donors, and in lung tissue of AoB rats relative to sham controls (**Fig. 12C,C'**).

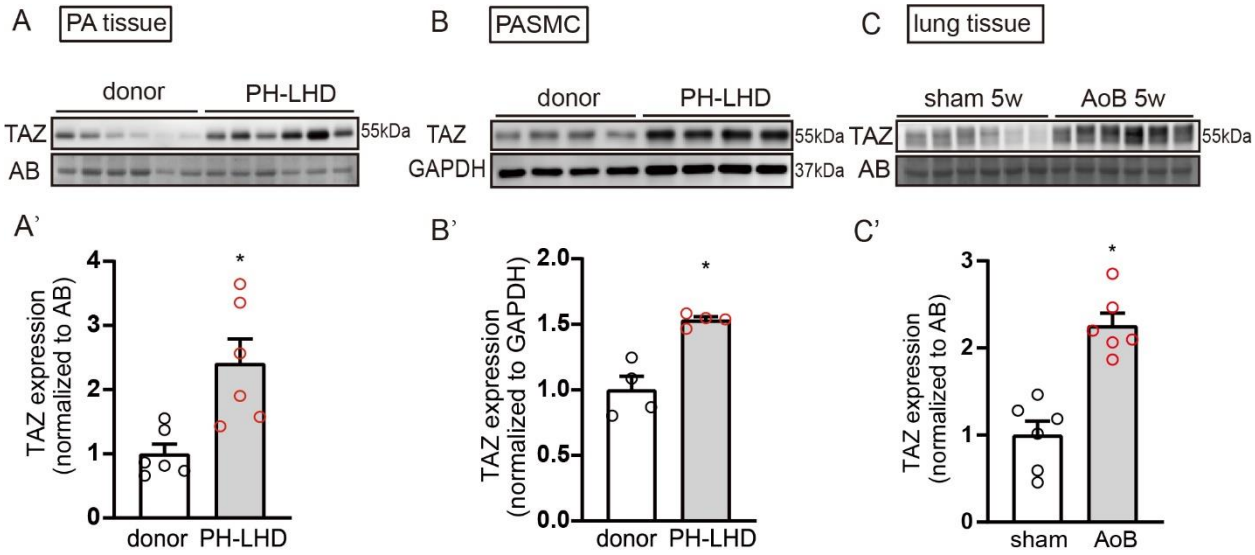

Figure 12. TAZ expression is upregulated in PH-LHD patients and AoB rats.

A-B) Representative western blots and (**A',B'**) corresponding densitometric quantification show protein expression of TAZ in PA (**A** and **A'**; n=6 per group) and isolated PAMSC (**B** and **B'**; n=4 per group) of PH-LHD patients compared with healthy-heart donors (*p<0.05 versus donor). **C**) Representative western blots and (**C'**) corresponding densitometric quantification of TAZ (n = 6, each group) show increased TAZ expression in lungs of AoB rats 5 weeks post-surgery as compared to corresponding sham controls (*p<0.05 versus sham). AB, amido black.

In parallel, immunofluorescence staining further revealed increased nuclear TAZ abundance in PA of PH-LHD patients (**Fig. 13A**) and AoB rats (**Fig. 13B**) relative to corresponding controls, respectively. As such, our data demonstrate increased TAZ expression and activation in PASMC in PH-LHD.

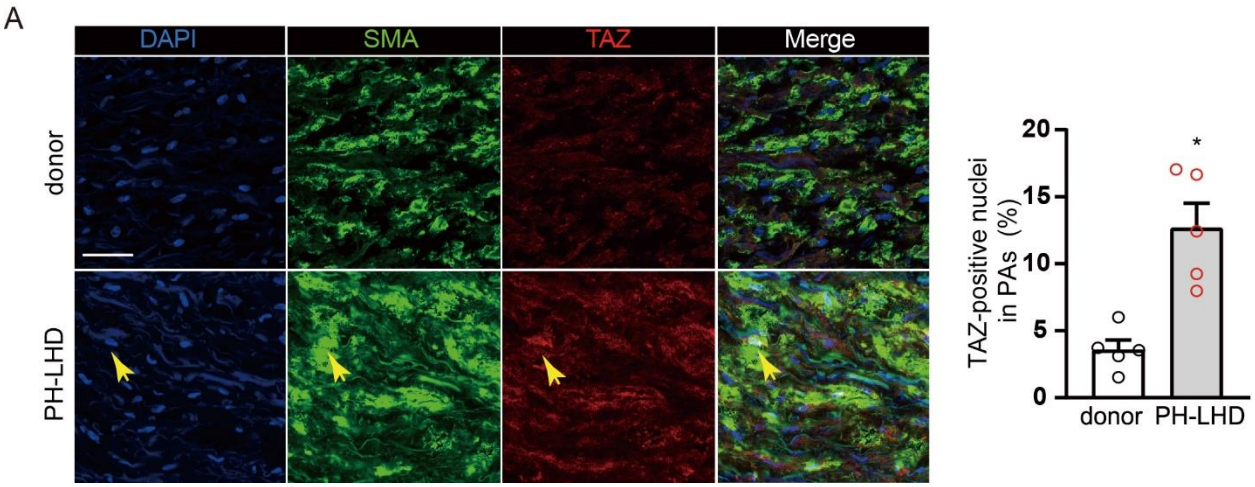

Figure 13 (continues on previous page)

B

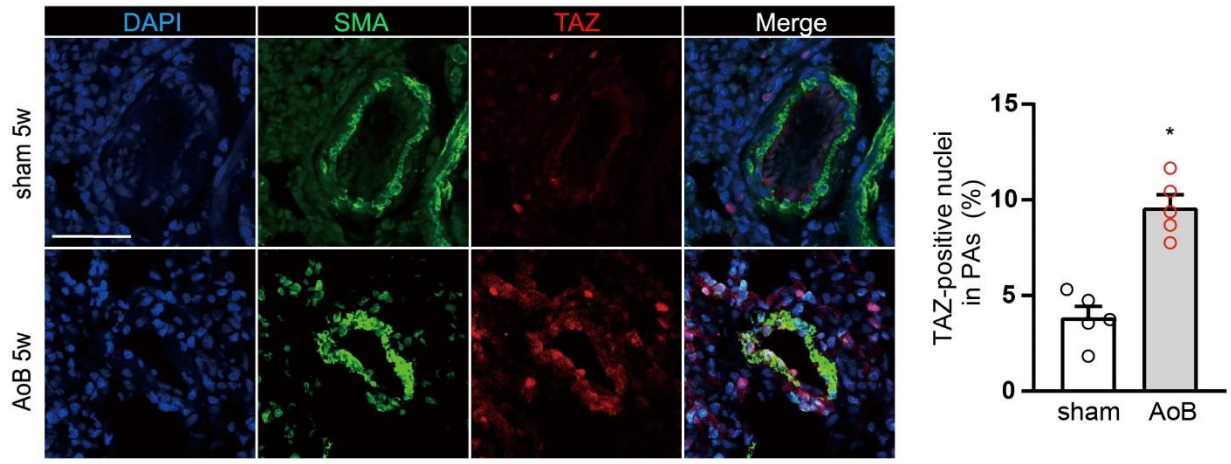

Figure 13. TAZ nuclear abundance is increased in PH-LHD patients and AoB rats.

A) Representative single z-plane fluorescence microscopic images of PASMC immunostained for TAZ (red) and α-SMA (green), and counterstained with DAPI (blue), and the corresponding quantification of TAZ positive nuclei in SMA-positive cells show an increased nuclear abundance of TAZ in PAs of PH-LHD patients as compared to healthy-heart donors (n=5 per group, scale bar: 50 µm, **p*<0.05 versus donor). **B**) Representative single z-plane fluorescence microscopic images of lung tissue immunostained for TAZ (red) and α-SMA (green), and counterstained with DAPI (blue), and the corresponding quantification of TAZ positive nuclei in PASMC of PAs show increased nuclear abundance of TAZ in PAs of AoB rats relative to sham (n = 5 rats per group; scale bar: 50 µm, **p*<0.05 versus sham).

3.6.2 TGF-β stimulation of PASMC replicates TAZ expression and activation

Next, we tested again whether TAZ upregulation and nuclear translocation identified in PA from PH-LHD patients and rats, respectively, could be replicated by TGF-β as a putative driver and *in vitro* surrogate stimulus of osteogenic transdifferentiation. Treatment of human PASMC with TGF-β upregulated TAZ expression at both the mRNA (**Fig. 14A**) and protein level (**Fig. 14B,B'**) within 72 hours. TGF-β treatment also increased the nuclear abundance of TAZ, as evidenced by immunoblotting of nuclear extracts (**Fig. 14C,C'**) and confirmed by immunofluorescence imaging (**Fig. 14D,D'**). These findings identify TGF-β as an activator of TAZ in PASMC that phenocopies the findings in PH-LHD.

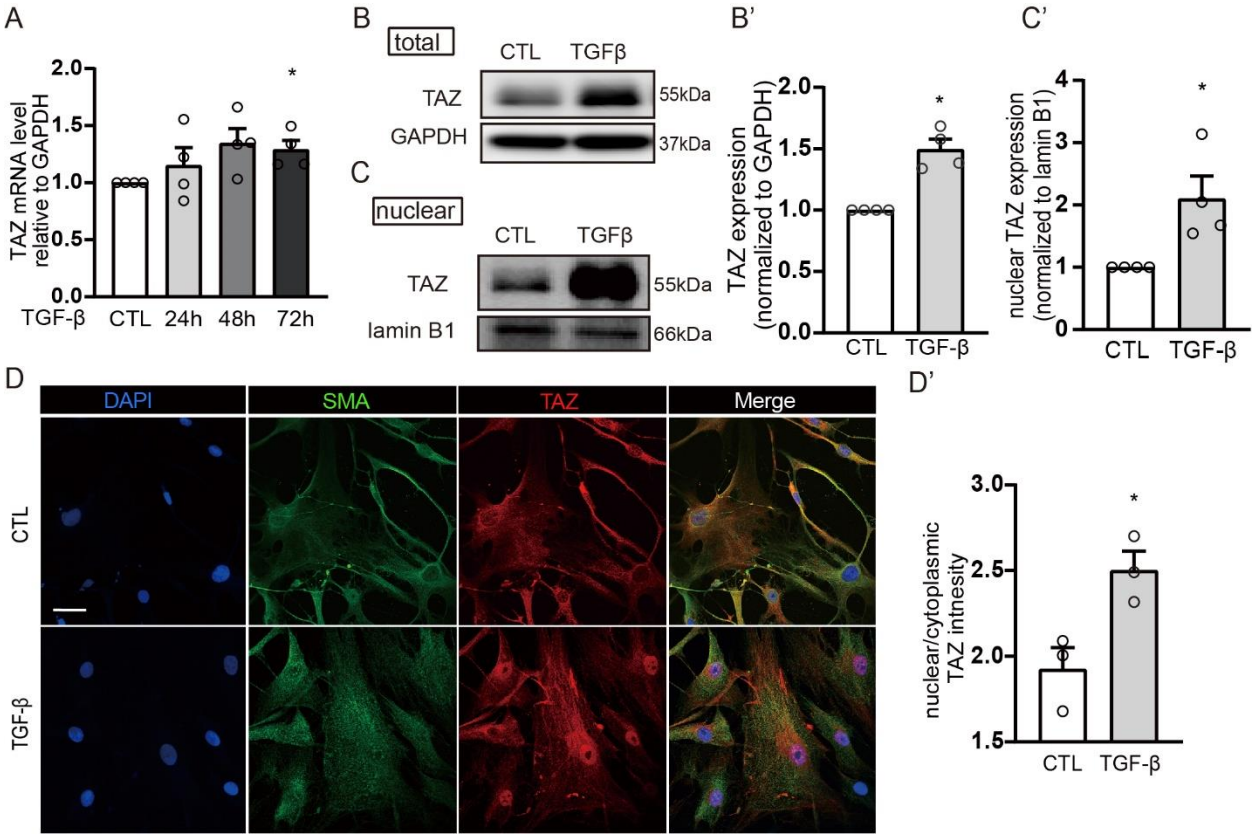

Figure 14. TAZ upregulation and nuclear localization in TGF-β treated PASMC.

A) mRNA expression levels as determined by real-time PCR show a time-dependent increase in TAZ expression in PASMC following stimulation with 10 ng/mL TGF-β or vehicle control (CTL) (n=4 biological replicates per group, *p<0.05 versus CTL). **B,C**) Representative western blots and (**B',C'**) corresponding densitometric quantification of TAZ protein expression (n=4 per group) show increased total (**B** and **B'**; n=4 per group) and nuclear (**C** and **C'**; n=4 per group) TAZ expression in human PASMC treated with TGF-β (10 ng/mL) for 72 hours (*p<0.05 versus CTL). **D**) Representative fluorescence microscopic images of PASMC immunostained for TAZ (red) and α-SMA (green), and counterstained with DAPI (blue), and the (**D'**) corresponding quantification of the nuclear-to-cytoplasmic ratio of TAZ fluorescence intensity show increased nuclear abundance of TAZ upon treatment with TGF-β (10 ng/mL for 72 hours) relative to controls (n=3 per group, scale bar: 50 µm, *p< 0.05 versus CTL).

3.7 RUNX2-TAZ protein-protein interaction protects RUNX2 from proteolytic degradation

3.7.1 RUNX2 is regulated by TAZ in PASMC

To probe for a potential regulation of RUNX2 by TAZ, we conducted a series of experiments in which we antagonized the effects of TAZ by two different interventions, either pharmacologically by use of the YAP/TAZ inhibitor Verteporfin [40], or at the genetic level

via TAZ-specific RNA silencing (siTAZ). Effective siRNA-mediated knockdown of TAZ in PASMC was verified by western blotting (**Fig. 15**).

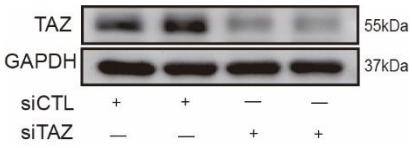

Figure 15. Effective siRNA-mediated knockdown of TAZ in PASMC.
Representative western blot shows decreased expression of TAZ in PASMC treated for 72 hours with a TAZ-specific siRNA (siTAZ) relative to a control siRNA (siCTL).

As was expected based on their mode of action, treatment with either Verteporfin or siTAZ decreased TAZ levels in PASMC. In parallel, both interventions also effectively prevented the TGF-β-induced increase in RUNX2 protein expression in PASMC (**Fig. 16A,B**). Consequently, these findings indicate a potential role for TAZ as a regulator of RUNX2 expression in PASMC, and suggest that targeting TAZ may present a viable strategy to mitigate osteogenic transdifferentiation of PASMC in PH-LHD.

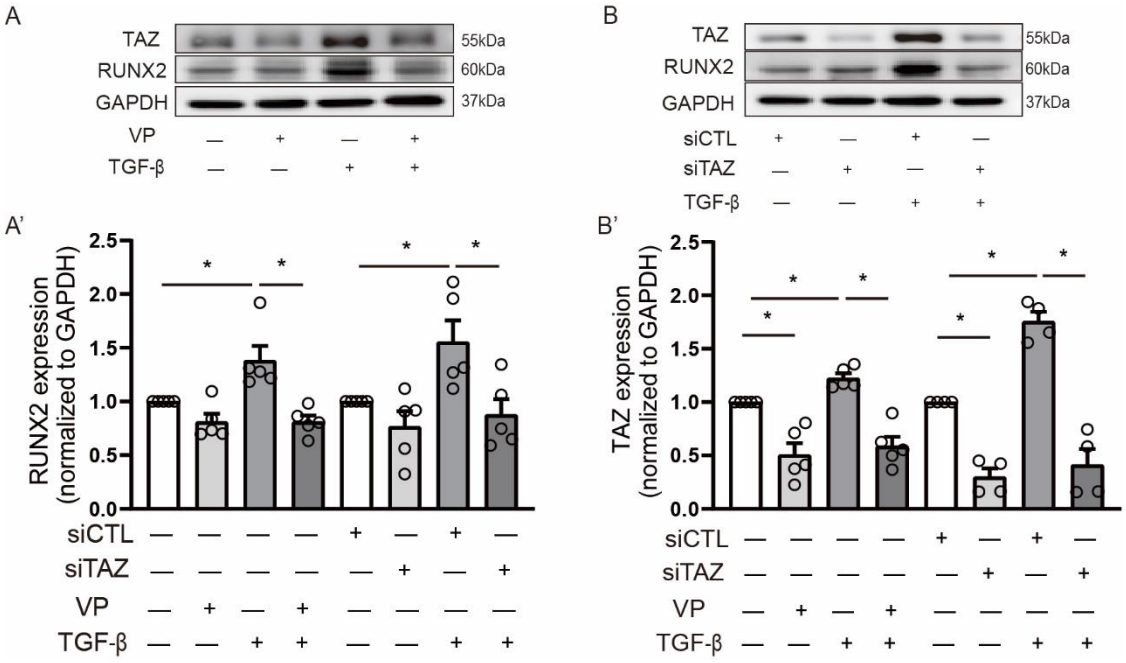

Figure 16. RUNX2 is regulated by TAZ in PASMC.
A,B) Representative western blots and corresponding densitometric quantification show decreased RUNX2 and TAZ expression in TGF-β (10 ng/mL for 72 hours) stimulated PASMC treated (**A**) with either the YAP/TAZ inhibitor Verteporfin (VP, 1 µMol/L for 24 hours) or (**B**) a TAZ-specific siRNA (siTAZ) relative to a control siRNA (siCTL; both for 72 hours) (n=4-5 biological replicates per group; *p<0.05).

3.7.2 TAZ regulates RUNX2 abundance at the protein rather than the mRNA level

Consistent with these results, Verteporfin treatment also reduced RUNX2 protein levels in PASMC isolated from patients with PH-LHD (**Fig. 17A**). Intriguingly, however, Verteporfin did not impact on the mRNA transcript level of RUNX2 (**Fig. 17B**). These findings suggest that TAZ may regulate RUNX2 expression at the post-transcriptional level, potentially via direct protein-protein interaction.

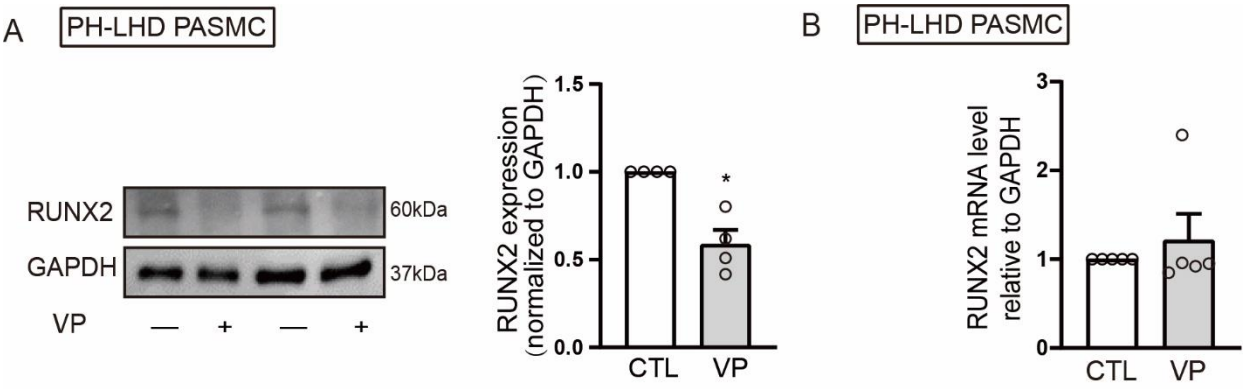

Figure 17. TAZ regulates RUNX2 abundance at the protein level.

A) Representative western blots and corresponding densitometric quantification (n=4 per group) show reduced RUNX2 protein expression in PASMC isolated from PH-LHD patients in response to Verteporfin (VP,1 µMol/L for 24 hours) relative to vehicle control (CTL) (n=4 per group; **p*<0.05 versus CTL). **B**) RUNX2 expression as measured by real-time PCR is unchanged after 24 hours VP treatment in PASMC isolated from PH-LHD patients (n=5 per group).

3.7.3 TAZ stabilizes RUNX2 via direct protein-protein interaction

To probe for a direct protein-protein interaction as a putative mechanism of the posttranslational regulation of RUNX2 abundance by TAZ, we performed co-immunoprecipitation experiments by pulling down RUNX2 and subsequently subjecting it to immunoblotting for TAZ. These experiments revealed a direct protein-protein interaction between RUNX2 and TAZ that was further enhanced by TGF-β treatment (**Fig. 18A,B**). Importantly, protein levels of both RUNX2 and TAZ in the precipitate increased in parallel, indicating that the observed increase in RUNX2-TAZ interaction upon TGF-β treatment reflects the increased abundance of both interaction partners, rather than a change in the affinity between the two proteins.

Based on the observed interaction between TAZ and RUNX2, as well as the reduced TGF-β-induced RUNX2 protein expression upon TAZ depletion by Verteporfin or siTAZ,

we hypothesized that TAZ may stabilize RUNX2 proteins, while loss of TAZ may accelerate RUNX2 degradation. We tested this concept in cycloheximide (CHX) chase experiments, in which we treated PASMC with TGF-β for 72 hours and the protein synthesis inhibitor cycloheximide (CHX, 5 µg/mL) for 6 hours. This allowed us to attribute any residual changes in protein levels to differences in the rate of protein degradation [41]. As was expected, CHX treatment reduced RUNX2 expression levels upon TGF-β stimulation, as it prevented the *de novo* synthesis of RUNX2 induced by TGF-β (**Fig. 18C**).

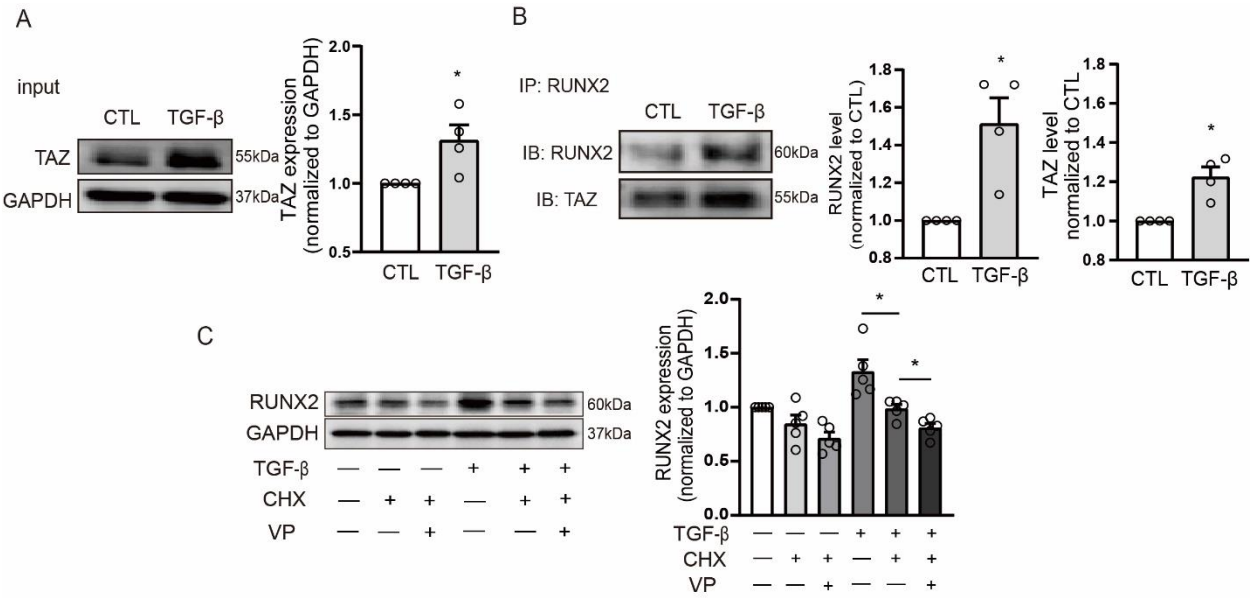

Figure 18. TAZ stabilizes RUNX2 via direct protein-protein interaction.

A,B) PASMC were treated with TGF-β (10 ng/mL) or vehicle (CTL) for 72 hours, immunoprecipitated (IP) using a RUNX2 antibody, and the precipitated pellets were immunoblotted (IB) for RUNX2 and TAZ. Representative western blots (**A**) and densitometric quantification of input prior to immunoprecipitation (**B**) and the immunoprecipitate reveal upregulation of both RunX2 and TAZ as well as increased co-immunoprecipitation (Co-IP) of both proteins upon TGF-β treatment (n=4 biological replicates, **p*<0.05 versus CTL). **C**) Representative western blots and corresponding quantification show increased RUNX2 degradation in the presence of Verteporfin (1 µMol/L for 6 hours) in a 6-hour cycloheximide (CHX, 5 µg/mL) chase assay (n=5 per group, **p*<0.05). VP, Verteporfin; CHX, cycloheximide.

3.7.4 TAZ binding decreases RUNX2 ubiquitination

The observed decrease in RUNX2 protein levels by Verteporfin in CHX chase experiments indicates that inhibition of the TAZ-RUNX2 interaction may accelerate the degradation of RUNX2, while conversely, the interaction between TAZ and RUNX2 stabilizes RUNX2. Consistent with this view, treatment of PASMC with the proteasome inhibitor

MG132 (10 µMol/L) increased the abundance of RUNX2 protein in the presence of Verteporfin (**Fig. 19A**). Ubiquitin pulldown and subsequent anti-RUNX2 immunoblotting additionally revealed increased levels of ubiquitinated RUNX2 upon TAZ inhibition (**Fig. 19B, C**). These findings collectively demonstrate the formation of a TAZ-RUNX2 complex in response to TGF-β which protects RUNX2 from ubiquitin-mediated proteasomal degradation.

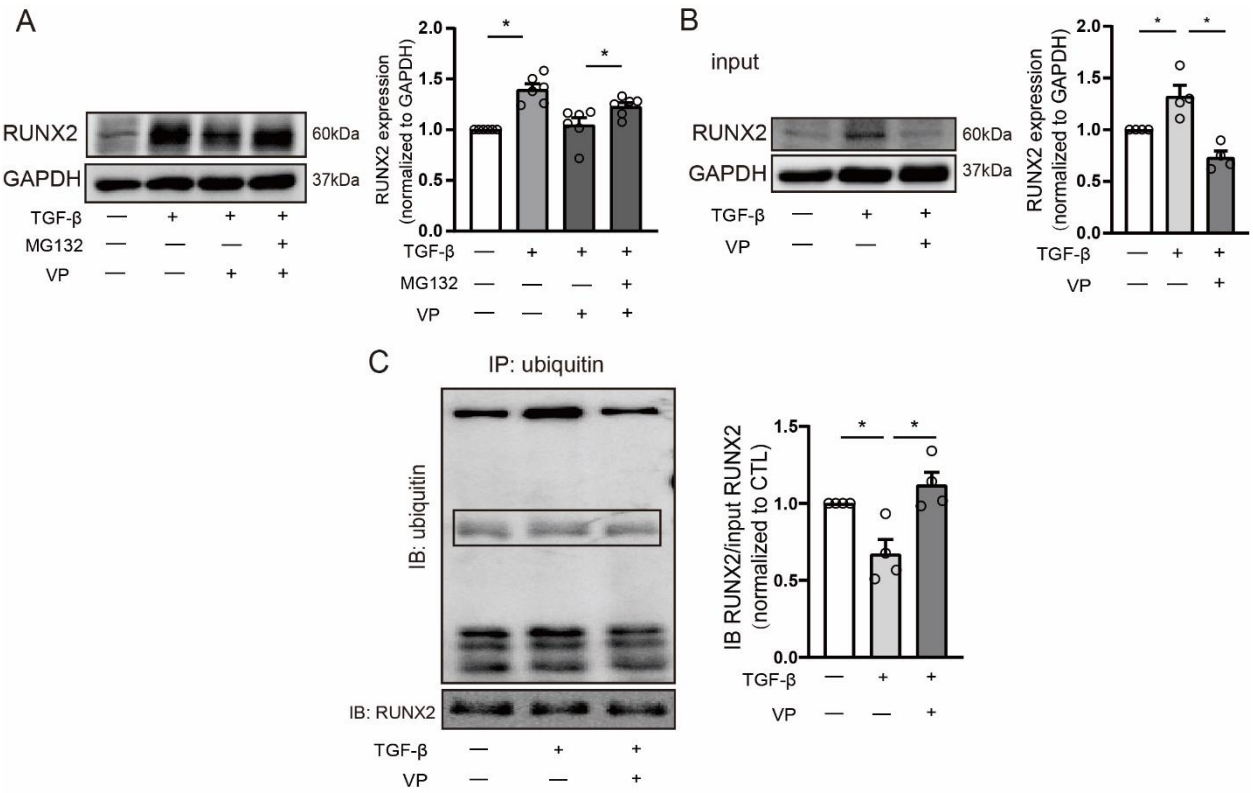

Figure 19. TAZ stabilizes RUNX2 by attenuating its ubiquitination and proteasomal degradation.

A) Representative western blots and corresponding quantification show increased RUNX2 protein abundance in PASMC in response to TGF-β treatment (10 ng/mL for 72 hours) that is attenuated by Verteporfin (VP, 1 µMol/L for 6 hours), yet partially rescued by the proteasome inhibitor MG132 (10 µMol/L for 6 hours) (n=6 per group, **p*<0.05). **B**) PASMC were treated with TGF-β (10 ng/mL) or vehicle (CTL) for 72 hours. After 66 hours, cells were treated with VP (1 µMol/L for 6 hours), then immunoprecipitated (IP) with an ubiquitin antibody, and the precipitated pellets were immunoblotted (IB) for ubiquitin and RUNX2. **C**) Representative western blots and densitometric quantification reveal increased co-immunoprecipitation (Co-IP) of RUNX2 with ubiquitin in Verteporfin-treated, TGF-β stimulated PASMC when corrected for reduced RUNX2 input in Verteporfin-treated cells (n=4 biological replicates, **p*<0.05).

3.7.5 TAZ inhibition decreases *in vitro* calcification in PASMC

As protein-protein interaction between TAZ and RUNX2 emerged as a critical determinant of RUNX2 abundance, we next probed for a potential consequential role of TAZ in vascular calcification. Inhibition of TAZ by Verteporfin decreased the calcified surface area in PASMC cultured *in vitro* in a calcification medium, both at baseline and in the presence of concurrent TGF-β stimulation (**Fig. 20A, A'**). Similarly, Verteporfin reduced the propensity for *in vitro* calcification of PASMC isolated from patients with PH-LHD (**Fig. 20B, B'**). These findings highlight a critical role for TAZ-RUNX2 interaction in vascular calcification, and identify TAZ-targeted strategies such as the clinically approved drug Verteporfin as potential therapeutic approach to mitigate calcification in PH-LHD.

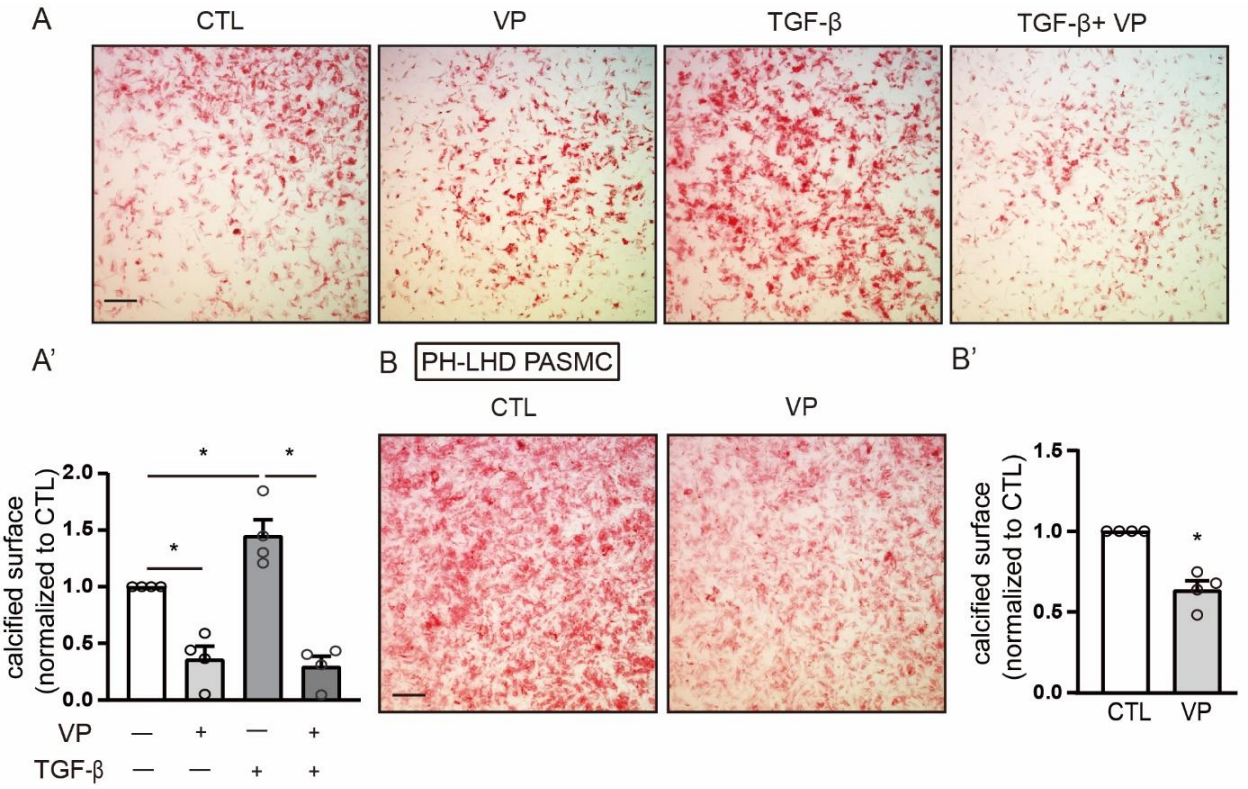

Figure 20. TAZ inhibition decreases *in vitro* calcification in PASMC.

A) Representative images and (**A'**) corresponding quantification show calcification (alizarin red stained area relative to control) in PASMC treated with TGF-β (10 ng/mL) or vehicle for 72 hours in calcification medium in the presence or absence of Verteporfin (VP,1 µM) (n=4 per group, scale bar: 50 µm, **p*<0.05). **B**) Representative images and (**B'**) corresponding quantification show calcification (alizarin red stained area relative to control) in PASMC isolated from PH-LHD patients and treated with VP (1 µMol/L) or vehicle for 72 hours in calcification medium (n=4 per group, scale bar: 50 µm, **p*<0.05 versus CTL).

3.8 RUNX2 inhibition attenuates lung vascular calcification and remodeling as well as normalizing RV hemodynamics in PH-LHD

To assess the functional contribution of RUNX2 to PA calcification and to probe whether RUNX2 may serve as putative target to prevent PA calcification in PH-LHD *in vivo,* we performed a therapeutic interventional study using CADD522, an inhibitor of RUNX2 binding to DNA [42], in our established preclinical model of PH-LHD. To this end, AoB rats were randomly assigned to receive either vehicle or CADD522 treatment. Treatment was administered biweekly through intraperitoneal injections over a period of 6 weeks, starting 3 weeks after AoB surgery or vehicle administration (**Fig. 21A**). Nine weeks after the surgery, untreated AoB rats exhibited characteristic signs of PH-LHD, as previously reported in this model [27]. Specifically, AoB rats displayed elevated left ventricular systolic pressures (LVSP, **Fig. 21B**) and right ventricular systolic pressures (RVSP, **Fig. 21C**), along with biventricular hypertrophy (as indicated by increased left ventricular and septal weight relative to body weight **(Fig. 21D)** and increased right ventricular weight relative to body weight (**Fig. 21E**)), a reduced right ventricular ejection fraction (RVEF, **Fig. 21F**) and tricuspid annular plane systolic excursion (TAPSE, **Fig. 21G**), a shorter pulmonary artery acceleration time (PAAT, **Fig. 21H**) and a reduced PA radial strain (PA RS, **Fig. 21I**) as echocardiographic parameters of RV dysfunction and PH as compared to sham-operated controls.

These characteristics of hemodynamic and structural cardiovascular deterioration were accompanied by histological evidence of vascular calcification, consistent with previous findings in this study. Specifically, calcium content was increased in lung tissue (**Fig. 21J**), and positive von Kossa staining indicated the presence of calcifications in the media of PAs (**Fig. 21K**). Additionally, medial wall thickening of distal pulmonary resistance vessels was prominent in AoB rats (**Fig. 21L**).

Consistent with a critical role of RUNX2 in PA calcification in PH-LHD, treatment with CADD522 from week 3 to week 9 post-AoB surgery reduced von Kossa staining in distal PA and decreased calcium content in lung tissue, indicating mitigated calcification. Importantly, CADD522 treatment also improved pulmonary and right ventricular (RV) hemodynamics, and normalized medial wall thickness in pulmonary arterioles. CADD522 did not, however, affect left ventricular (LV) hypertension and hypertrophy following AoB surgery (**Fig. 21B-I**). Notably, CADD522 treatment had no discernible effect on hemodynamics or histological features in sham-operated rats. These findings not only confirm the

critical role of RUNX2 in PA calcification, but also suggest that subsequent PA stiffening acts as an important driver of both downstream pulmonary vascular remodeling and upstream RV dysfunction.

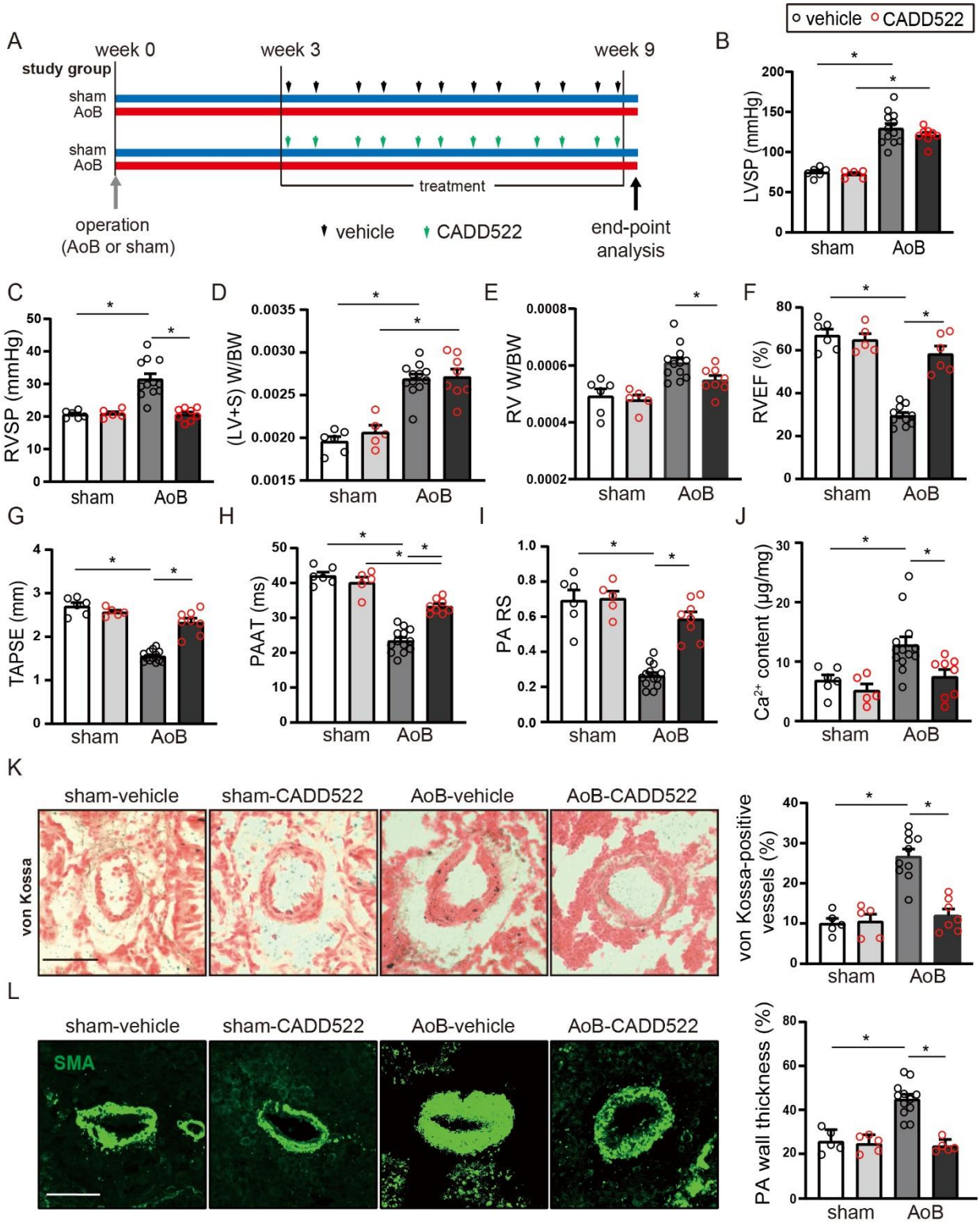

Figure 21. RUNX2 inhibition attenuates lung vascular calcification and remodeling in AoB rats.

A) Experimental protocol for RUNX2 inhibition in rats with aortic banding (AoB)-induced PH-LHD or in sham-operated controls. CADD522 (10 mg/kg body weight) was given biweekly by intraperitoneal injection

starting 3 weeks post-AoB for 6 weeks (until week 9), at which time end-point hemodynamic and histological assessments were performed. Quantitative data show (**B**) left (LVSP) and (**C**) right ventricular systolic pressure (RVSP) as determined by cardiac catheterization, and (**D**) left and (**E**) right ventricular hypertrophy, determined as the weight of the left ventricle plus septum (LV+S) or the right ventricle (RV) relative to body weight (BW), respectively. Echocardiographic analyses yielded (**F**) right ventricular ejection fraction (RVEF), (**G**) tricuspid annular plane systolic excursion (TAPSE), (**H**) pulmonary artery acceleration time (PAAT), and (**I**) pulmonary artery radial strain (PA RS). **J**) Quantitative data show Ca^{2+} content in lung tissue (panels b-j: n=5–13 rats per group; **p*<0.05). **K**) Representative images and quantitative data show reduced calcification of pulmonary arteries in AoB rats treated with CADD522, as determined by the fraction of von Kossa-positive vessels in distal PA (n=5–10 rats per group, scale bar: 50 µm, **p*<0.05). **L**) Representative fluorescence microscopic images of distal PA immunostained for α-SMA (green) and corresponding quantification show reduced vascular wall thickness of pulmonary arterioles in AoB rats treated with CADD522 (n=5–12 rats per group, scale bar: 50 µm, **p*<0.05).

3.9 TAZ inhibition phenocopies the effects of RUNX2 inhibition on lung vascular calcification, remodeling, and RV hemodynamics in PH-LHD

Based on our previous findings that demonstrated i) the ability of Verteporfin to accelerate RUNX2 degradation and attenuate PASMC calcification in response to TGF-β *in vitro*, and ii) the therapeutic effect of CADD522 on vascular calcification, as well as pulmonary and right ventricular hemodynamics in preclinical PH-LHD, we aimed to test for a similar protective effect of the YAP/TAZ inhibitor Verteporfin on hemodynamic and structural alterations in our rat AoB model. Analogously to CADD522, Verteporfin was delivered biweekly via intraperitoneal injection over 6 weeks from weeks 3 to 9 post-AoB surgery (**Fig. 22A**).

Analogously to the effects of RUNX2 inhibition, AoB rats treated with Verteporfin demonstrated significant improvement in pulmonary and right ventricular hemodynamics, as well as a reduction in right ventricular hypertrophy. Moreover, these rats showed reduced vascular calcification, lung calcium content, and arteriolar wall thickness compared to vehicle-treated AoB rats (**Fig. 22B-L**). Consequently, these findings further support the mechanistic link between TAZ and RUNX2 in PA calcification, highlight the beneficial effects of targeting PA calcification on lung hemodynamics and vascular remodeling in PH-LHD, and identify RUNX2 and TAZ as putative therapeutic targets for the prevention or treatment of PH-LHD.

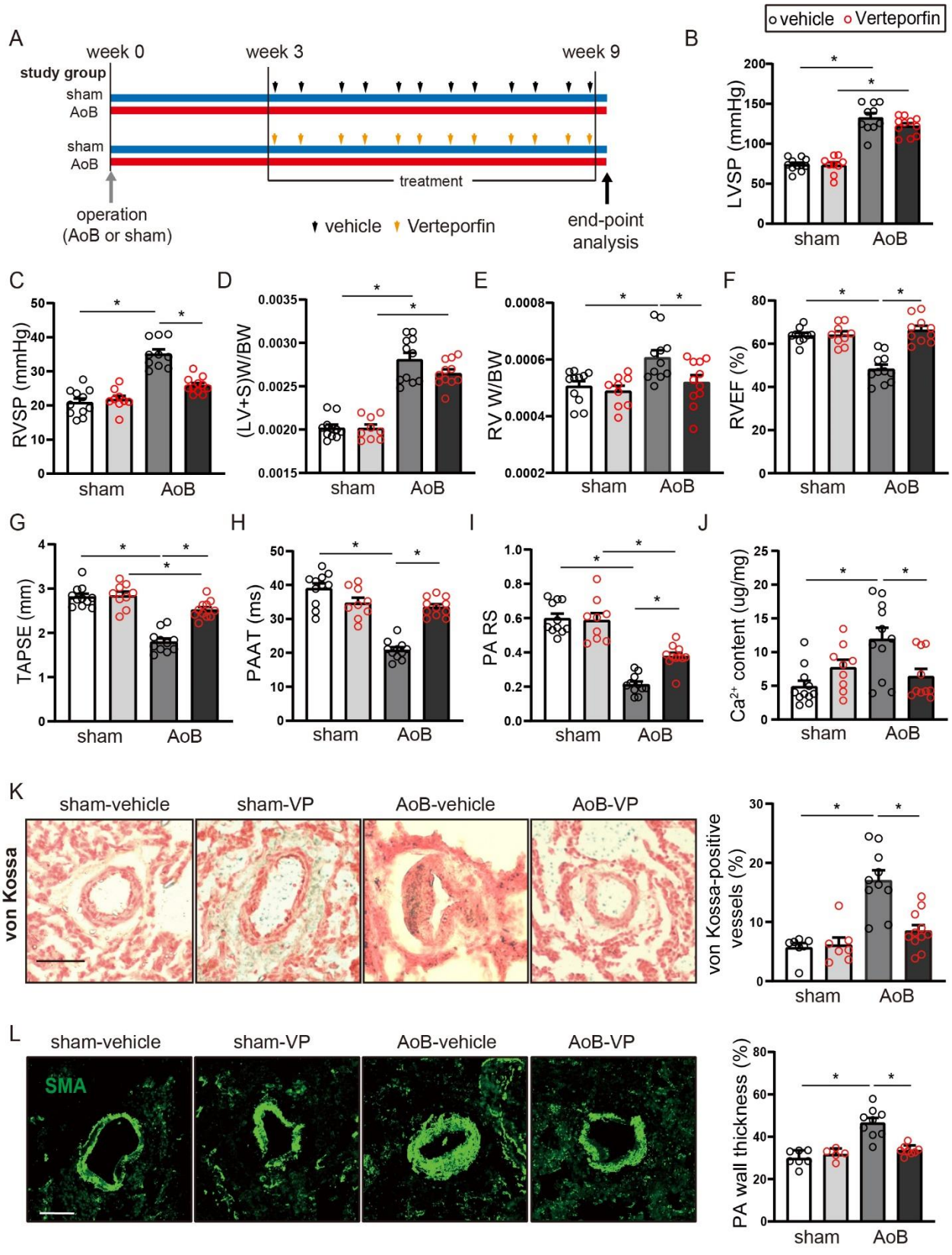

Figure 22. TAZ inhibition attenuates lung vascular calcification and remodeling in rats.

A) Experimental protocol for Verteporfin treatment in rats with aortic banding (AoB)-induced PH-LHD or in sham-operated controls. Verteporfin (10 mg/kg body weight) was given biweekly by intraperitoneal injection starting 3 weeks post-AoB for 6 weeks (until week 9), at which time end-point hemodynamic and histological

assessments were performed. Quantitative data show (**B**) left (LVSP) and (**C**) right ventricular systolic pressure (RVSP) as determined by cardiac catheterization, and (**D**) left and (**E**) right ventricular hypertrophy, determined as the weight of the left ventricle plus septum (LV+S) or the right ventricle (RV) relative to body weight (BW), respectively. Echocardiographic analyses yielded (**F**) right ventricular ejection fraction (RVEF), (**G**) tricuspid annular plane systolic excursion (TAPSE), (**H**) pulmonary artery acceleration time (PAAT), and (**I**) pulmonary artery radial strain (PA RS). **J**) Quantitative data show Ca^{2+} content in lung tissue (panels b-j: n=9–11 rats per group; **p*<0.05). **K**) Representative images and quantitative data show reduced calcification of pulmonary arteries in AoB rats treated with Verteporfin, as determined by the fraction of von Kossa-positive vessels in distal PA (n=7–11 rats per group, scale bar: 50 µm, **p*<0.05). **L**) Representative fluorescence microscopic images of distal PA immunostained for α-SMA (green) and corresponding quantification show reduced vascular wall thickness of pulmonary arterioles in AoB rats treated with Verteporfin (n=5–9 rats per group, scale bar: 50 µm, **p*<0.05).

4. Discussion

4.1 Summary of the Results

In the present study, we i) identify vascular calcification as a characteristic feature of remodeled PA in patients with PH-LHD and in a corresponding animal model in rats, ii) delineate the underlying signaling pathway involving TGF-β, TAZ, and RUNX2, and iii) demonstrate the therapeutic potential of targeting PA calcification for mitigating vascular remodeling and alleviating hemodynamic deterioration in PH-LHD (**Fig. 23**).

Specifically, our study reveals that upregulation and activation of the osteogenic transcription factor RUNX2 in PASMC drives vascular calcification and the expression of osteogenic markers in PH-LHD. We successfully replicated these effects *in vitro* by treating PASMC with TGF-β, a key regulator of lung vascular remodeling that was found to be elevated in PH-LHD patients. PH-LHD in patients or *ex vivo* treatment with TGF-β also increased the expression and nuclear abundance of the HIPPO pathway transcriptional co-activator TAZ, which was shown to stabilize RUNX2 via direct protein-protein interaction, preventing its degradation via ubiquitination and proteasomal degradation, thus increasing the abundance of this transcription factor. Finally, pharmacological inhibition of either RUNX2 or TAZ in rats with established PH-LHD not only prevented PA calcification but also reduced distal pulmonary vascular remodeling, while simultaneously normalizing PA and right ventricular hemodynamics. These findings highlight the potential of targeting vascular calcification and its underlying signaling pathways as promising therapeutic strategies for the treatment of PH-LHD.

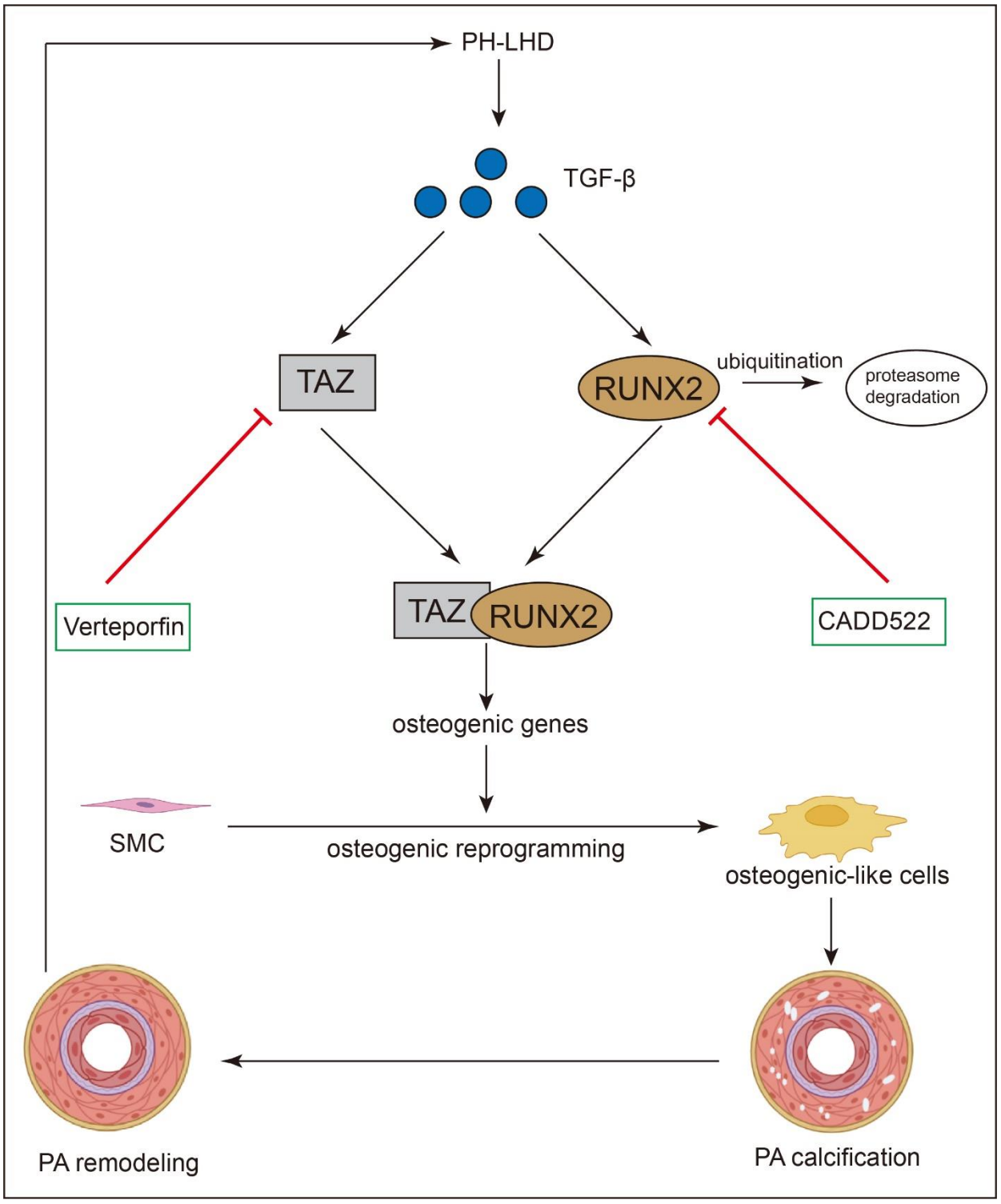

Figure 23. Proposed signaling pathway of PA calcification in PH-LHD.

In pulmonary hypertension due to left heart disease (PH-LHD), elevated levels of circulating transforming growth factor-β (TGF-β) – likely to be in conjunction with mechanosensitive signaling pathways (not shown) – drive increased expression and activation of the HIPPO transcriptional co-activator TAZ and the osteogenic transcription factor RUNX2 in pulmonary artery smooth muscle cells (PASMC). TAZ and RUNX2 form a complex which stabilizes RUNX2 by preventing its degradation via the ubiquitin-proteasomal pathway. RUNX2 then drives osteogenic reprogramming of PASMC characterized by expression of osteogenic

genes and progressive calcification of pulmonary artery (PA). PA calcification promotes distal vessel remodeling which in turn aggravates PH-LHD, thus establishing a detrimental feedback loop that can be intercepted, however, by pharmacological inhibition of either TAZ or RUNX2, respectively. Verteporfin: TAZ inhibitor; CADD522: RUNX2 inhibitor.

4.2 PA calcification in PH-LHD

Traditionally, vascular calcification has been considered as a prominent pathological feature of systemic arteries in cardiovascular diseases including atherosclerosis, diabetes, or hypertension [4]. Recently, vascular calcification has also been reported in the pulmonary circulation - specifically, in pulmonary arteries of patients with pulmonary arterial hypertension (PAH) [15]. This finding was subsequently validated by non-contrast thoracic CT scans showing an increased radiodensity in pulmonary arteries, indicating early vascular calcification in PAH patients [43]. Analogously, pulmonary artery (PA) calcification has been demonstrated in rodent models of monocrotaline (MCT)-induced or chronic hypoxic PH [44, 45]. To our knowledge, however, the present study is the first to demonstrate pulmonary arterial calcification in both the proximal and distal PA in group 2 pulmonary hypertension (PH), also known as PH due to left heart disease (PH-LHD). Given the distinct pathogenesis of PH-LHD compared to PAH or chronic hypoxic PH, this finding is particularly relevant considering the high prevalence of PH-LHD, which accounts for 65-80% of all PH cases [1]. PA calcification in PH-LHD was initially identified by sequencing analyses and subsequently confirmed by histological analyses using von Kossa and alizarin red staining for calcium deposition and colorimetric measurement of calcium content in the pulmonary artery of PH-LHD patients and in a corresponding rat model of PH-LHD secondary to AoB. Von Kossa staining is utilized for the detection of calcium phosphate deposition in tissues, with black precipitate marking fine calcium salt deposits. In contrast, alizarin red staining forms red chelates with calcium ions to reveal the deposition of calcium salts in tissues. In comparison to the black von Kossa staining, alizarin red is, however, commonly harder to detect against the tissue background, and as such, often less sensitive for the detection of subtle calcifications. This may explain the absence of a positive alizarin red signal at 5 weeks post-AoB surgery in spite of a notable von Kossa staining.

4.3 TGF-β regulated RUNX2 and TAZ complex formation as a critical driver of PA calcification in PH-LHD

Nuclear translocation of RUNX2 is a critical step in the osteogenic transformation of smooth muscle cells and the initiation of vascular calcification [46]. In the present study, RUNX2 translocation was evident in both PA and PASMC isolated from PH-LHD patients, as well as in lung tissue of PH-LHD rats. Upregulation of the bone marker proteins osterix and alkaline phosphatase, which are regulated by RUNX2, further confirmed osteogenic transformation in the respective tissues and cells. As such, the process of PA calcification in PH-LHD resembles the RUNX2-mediated osteoblastic differentiation of vascular smooth muscle cells observed in systemic vessel in diseases such as chronic kidney disease [47], diabetes [48] or atherosclerosis [13, 49].

In PH-LHD, the expression and activation of RUNX2 in PASMC are likely to be regulated by multiple mechanisms which often prove difficult to replicate *in vitro*. In the present study, we specifically focused on the potential role of TGF-β, given its central involvement in lung vascular remodeling [33], its ability to induce RUNX2 expression [37, 38], and the subsequent activation of RUNX2-dependent osteoblast-specific gene expression [37, 38]. Notably, TGF-β has previously been reported to be abundant in serum and pulmonary vessels in AoB rats [25]. Consistent with these findings, we detected elevated levels of both TGF-β monomer and the mature TGF-β dimer in the plasma of PH-LHD patients relative to healthy-heart donors. Mature TGF-β dimer was also detected in the plasma, and latent TGF-β in lung tissues of AoB rats, in line with previous reports [25].

In our *in vitro* experiments, we show that stimulation of PASMC with TGF-β increases protein expression and nuclear translocation of RUNX2, as well as calcification of PASMC. As such, TGF-β replicates the PASMC phenotype in PH-LHD and may contribute relevantly to PA calcification in PH-LHD *in vivo*. By using TGF-β as an *in vitro* surrogate stimulus to mimic PASMC osteogenic differentiation in PH-LHD, we further investigated the molecular mechanisms underlying the regulation of RUNX2 in PH-LHD, with a specific focus on the interaction between RUNX2 and the transcriptional HIPPO pathway co-activator TAZ based on the previous recognition that RUNX2 and TAZ can form a master transcription factor complex in osteoblastogenesis [20].

Considering the high sensitivity of TAZ signaling to mechanical cues [21], such an interaction is an attractive candidate scenario for PH-LHD where increased lung vascular pressure constitutes the main driving force for lung vascular remodeling. It is, however,

worth noting that we also had to take the opposite scenario in consideration, where TAZ would exert a protective effect against vascular calcification. Specifically, recent studies have shown that YAP/TAZ can bind Disheveled 3 (DVL3) in the cytosol, preventing its nuclear translocation and subsequent osteogenic differentiation of vascular smooth muscle cells [50]. As such, the role of YAP/TAZ in vascular calcification is likely to be multifaceted and may vary depending on the specific cell type, stimulus, and biochemical or biomechanical context. In our study, we observed increased protein expression and nuclear localization of TAZ in PA and isolated PASMC of PH-LHD patients. Similar to the findings on RUNX2, the response of TAZ in PH-LHD patients was also replicated in AoB rats *in vivo*, and by TGF-β simulation of PASMC *in vitro*. The latter finding is in line with recent studies in kidney fibroblasts and epithelial cells that have shown upregulation of TAZ, but not YAP, by TGF-β through the myocardin-related transcription factor (MRTF) [21]. To investigate the functional impact of TAZ on RUNX2 expression and its downstream effects on vascular calcification, we employed two experimental strategies to downregulate TAZ: siRNA-mediated knockdown and treatment with the photosensitizer Verteporfin. In an *in vitro* screen, Verteporfin was initially identified as an inhibitor of the interaction between the transcriptional co-activators YAP and TAZ with their respective transcription factor TEA domain (TEAD) independent of light activation [51]. As such, Verteporfin downregulates YAP/TAZ expression by a mechanism that is not yet fully resolved [52, 53], but which was similarly evident in the present study. In our work, we found that TAZ deficiency in response to either Verteporfin or siRNA-mediated silencing results decreased protein levels of RUNX2 in TGF-β stimulated PASMC as well as in primary PASMC isolated from PH-LHD patients. Interestingly, treatment with Verteporfin did not affect RUNX2 mRNA levels in primary PASMC of PH-LHD patients, suggesting that TAZ regulates the abundance of RUNX2 protein at the post-translational level.

To investigate potential mechanisms underlying the TAZ-mediated regulation of RUNX2, we performed immunoprecipitation and CHX chase assays. These experiments revealed a protein-protein interaction between TAZ and RUNX2, whereby TAZ binds to RUNX2 and protects it from ubiquitination and subsequent degradation by the proteasome. This interaction was observed both at baseline and, to a greater extent, following TGF-β stimulation, presumably due to the elevated expression levels of both RUNX2 and TAZ. Depletion of TAZ by Verteporfin reduced RUNX2 protein abundance in TGF-β stimulated PASMC, especially in the presence of the protein synthesis inhibitor CHX [54], indicating

that TAZ may stabilize RUNX2 via their protein-protein interaction. Consistent with this notion, inhibition of proteasome activity with MG132 rescued the expression of RUNX2 in Verteporfin-treated, TGF-β stimulated PASMC, while Verteporfin treatment increased the ubiquitination of RUNX2 in TGF-β stimulated PASMC.
Based on these findings, we propose a novel role for the TAZ-RUNX2 transcription factor complex as a stabilizer of RUNX2 protein levels. Depletion of TAZ by Verteporfin disrupts this complex, leading to destabilization and degradation of RUNX2. These data implicate that Verteporfin may counteract RUNX2-mediated vascular calcification, a notion that was subsequently confirmed in both TGF-β stimulated PASMC and primary PASMC isolated from PH-LHD patients, in which Verteporfin attenuated calcification *in vitro*.

4.4 Limitations of the study and areas of future research

In the interpretation of the present study, several potential limitations should be considered. First, the analysis of distal vessel calcification and remodeling was limited to our *in vivo* animal model, as only tissue samples from proximal PA of PH-LHD patients could be obtained during cardiac transplantation and, thus, only these were available for examination. Therefore, direct assessment of distal vessel involvement in PH-LHD patients remains an area for future investigation.

Second, it is important to note that Verteporfin, the pharmacological intervention used in the present study to downregulate TAZ, also has an effect on YAP. While YAP and TAZ are closely related proteins, they have distinct functions in the vasculature, in that YAP primarily regulates the formation and maintenance of blood vessels [55], while TAZ has been implicated in vascular calcifications and the expression of genes involved in the formation of hydroxyapatite, a major component of calcified tissue [20]. In our study, we focused specifically on the role of TAZ in the context of PH-LHD. However, the potential contribution of YAP to the observed effects should not be disregarded and warrants further investigation.

Furthermore, we considered that PA calcification in PH-LHD patients may also be partially linked to chronic kidney disease, as the eGFR levels in this cohort were below the normal range of 90-120 mL/min·1.73 m^2 (**Table 1)**. This finding is not surprising considering the high prevalence of renal dysfunction in all types of heart failure [56]. However, it is important to note that eGFR by itself did not show a correlation with PA calcium content,

while patients with apparently normal eGFR levels had PA calcium levels at the upper end of the normal range or beyond (**Fig. 24**), as defined in healthy heart donors (**Fig. 5E**). We conclude from these data that although chronic kidney disease may contribute to the aggravation of PA calcification in PH-LHD, it is not the primary cause.

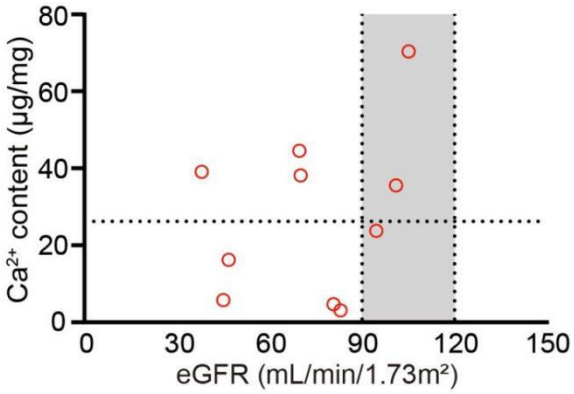

Figure 24. PA calcium content is not associated with eGFR in PH-LHD patients.
Dot plot shows relation between estimated glomerular filtration rate (eGFR) and PA calcium content in PH-LHD patients (n=10). The vertical shaded area represents the normal range for eGFR, and the horizontal dotted line indicates the upper limit of normal for PA calcium content defined as mean+2SDs calculated from donor group data shown in Figure 5E. Pearson's correlation analysis revealed no significant association between eGFR and PA calcium content (r=0.32, p=0.36).

Furthermore, we need to consider that the effects of the RUNX2 inhibitor CADD522 or the TAZ inhibitor VP on pulmonary hemodynamics and distal lung vascular remodeling in AoB rats may not be solely attributable to reduced vascular calcification. Both RUNX2 and TAZ have been shown to regulate the proliferation of vascular cells independent of their osteogenic transdifferentiation [15, 57]. As such, calcification-independent effects may have contributed to the therapeutic effectiveness of both interventions. Importantly, this recognition does not take away from the translational promise of targeting RUNX2 and/or TAZ for the prevention or treatment of PH-LHD.

Lastly, it is plausible that in addition to TGF-β and biomechanical cues, epigenetic factors such as non-coding RNAs contribute to the regulation of transcription factors like RUNX2 and TAZ in PH-LHD. In line with this notion, previous work by Ruffenach and colleagues demonstrated negative regulation of RUNX2 by the microRNA miR-204 in PASMC, with loss of miR-204 driving RUNX2-mediated calcification and remodeling of pulmonary arteries in the context of PAH [15]. For the unique scenario of PH-LHD, a similar epigenetic regulation is so far unclear and awaits exploration in future studies.

4.5 Clinical implications

The *in vivo* relevance of the newly identified TAZ-RUNX2 signaling pathway in vascular calcification was demonstrated by targeted pharmacological interventions in AoB rats. Treatment with CADD522, an inhibitor of RUNX2-DNA binding [42], and Verteporfin, an inhibitor of TAZ's interaction with its corresponding transcription factor TEAD, attenuated histological signs of vascular calcification, reduced lung tissue calcium content, and improved PA stiffness *in vivo* as indicated by normalization of PA RS in the echocardiographic assessment. Importantly, both interventions also improved hemodynamic parameters, echocardiographic measurements, and morphological characteristics of pulmonary hypertension and right ventricular dysfunction in AoB rats, as well as histological evidence of distal vessel remodeling. As such, these findings highlight the critical role of vascular calcification as a promoter of both upstream and downstream cardiovascular pathology in PH-LHD. Increased PA stiffness contributes to elevated right ventricular afterload through increased pulse pressure and impedance, while distal vessel disease is aggravated by accelerated pulse wave transmission, higher shear stress, and the subsequent development of a detrimental mechanobiological feedback [58]. As a result, vascular calcification and PA stiffening emerge as early events in the progression of PH-LHD and represent attractive therapeutic targets for its treatment.

Notably, Verteporfin is of particular interest in this context, as it is already approved for clinical use as a photosensitizer in the treatment of abnormal retinal vessels in conditions such as macular degeneration [59]. While Verteporfin has demonstrated anti-fibrotic effects in various organs, including the lungs, in preclinical animal models [60], and has been suggested as a locally administered drug for scar prevention [61], its chronic systemic application in humans has not yet been attempted, and is complicated by its photosensitization properties.

Our present findings highlight the potential of vascular calcification and its underlying signaling pathways as a promising therapeutic target for the treatment and/or prevention of PH-LHD, with Verteporfin holding promise as a candidate for further investigation due to its already established clinical use and demonstrated effects on TAZ signaling. However, additional research and careful consideration of the challenges associated with its systemic application are necessary before its potential as a treatment option for PH-LHD can be fully evaluated.

5. Conclusions

Our study reveals PA calcification, and its underlying regulation via TAZ and RUNX2, as a characteristic of PH-LHD that contributes relevantly to the remodeling of distal pulmonary vessels and impaired pulmonary artery and right ventricular hemodynamics. As such, identification of vascular calcification, whether through non-contrast thoracic CT scans or analysis of PA samples obtained during heart transplantation, holds promise as an important diagnostic and prognostic biomarker in patients with LHD that may accurately identify individuals at increased risk for developing PH. Implementing the assessment of vascular calcification as part of clinical evaluations may aid in early detection and intervention, ultimately improving patient outcome in the management of PH-LHD.

Reference list

1. Humbert M, Kovacs G, Hoeper MM, Badagliacca R, Berger RMF, Brida M, Carlsen J, Coats AJS, Escribano-Subias P, Ferrari P, Ferreira DS, Ghofrani HA, Giannakoulas G, Kiely DG, Mayer E, Meszaros G, Nagavci B, Olsson KM, Pepke-Zaba J, Quint JK, Rådegran G, Simonneau G, Sitbon O, Tonia T, Toshner M, Vachiery JL, Vonk Noordegraaf A, Delcroix M, Rosenkranz S; ESC/ERS Scientific Document Group. 2022 ESC/ERS Guidelines for the diagnosis and treatment of pulmonary hypertension. *Eur Respir J*. 2023 Jan 6;61(1):2200879. doi: 10.1183/13993003.00879-2022
2. Vachiéry JL, Tedford RJ, Rosenkranz S, Palazzini M, Lang I, Guazzi M, Coghlan G, Chazova I, De Marco T. Pulmonary hypertension due to left heart disease. *Eur Respir J*. 2019 Jan 24;53(1):1801897. doi: 10.1183/13993003.01897-2018
3. Breitling S, Ravindran K, Goldenberg NM, Kuebler WM. The pathophysiology of pulmonary hypertension in left heart disease. *Am J Physiol Lung Cell Mol Physiol*. 2015 Nov 1;309(9):L924-41. doi: 10.1152/ajplung.00146.2015
4. Demer LL, Tintut Y. Vascular calcification: pathobiology of a multifaceted disease. *Circulation*. 2008 Jun 3;117(22):2938-48. doi: 10.1161/CIRCULATIONAHA.107.743161
5. Yahagi K, Kolodgie FD, Lutter C, Mori H, Romero ME, Finn AV, Virmani R. Pathology of Human Coronary and Carotid Artery Atherosclerosis and Vascular Calcification in Diabetes Mellitus. *Arterioscler Thromb Vasc Biol*. 2017 Feb;37(2):191-204. doi: 10.1161/ATVBAHA.116.306256
6. Van Campenhout A, Golledge J. Osteoprotegerin, vascular calcification and atherosclerosis. *Atherosclerosis*. 2009 Jun;204(2):321-9. doi: 10.1016/j.atherosclerosis.2008.09.033
7. Reiss AB, Miyawaki N, Moon J, Kasselman LJ, Voloshyna I, D'Avino R, Jr., De Leon J. CKD, arterial calcification, atherosclerosis and bone health: Inter-relationships and controversies. *Atherosclerosis.* 2018 Nov;278:49-59. doi: 10.1016/j.atherosclerosis.2018.08.046
8. Moe SM, Chen NX. Inflammation and vascular calcification. *Blood Purif*. 2005;23(1):64-71. doi: 10.1159/000082013

9. Nikolovski J, Kim BS, Mooney DJ. Cyclic strain inhibits switching of smooth muscle cells to an osteoblast-like phenotype. *FASEB J*. 2003 Mar;17(3):455-7. doi: 10.1096/fj.02-0459fje
10. Liu SF, Nambiar Veetil N, Li Q, Kucherenko MM, Knosalla C, Kuebler WM. Pulmonary hypertension: Linking inflammation and pulmonary arterial stiffening. *Front Immunol*. 2022 Oct 5;13:959209. doi: 10.3389/fimmu.2022.959209
11. Ducy P. Cbfa1: a molecular switch in osteoblast biology. *Dev Dyn*. 2000 Dec;219(4):461-71. doi: 10.1002/1097-0177(2000)9999:9999<::AID-DVDY1074>3.0.CO;2-C.
12. Speer MY, Li X, Hiremath PG, Giachelli CM. Runx2/Cbfa1, but not loss of myocardin, is required for smooth muscle cell lineage reprogramming toward osteochondrogenesis. *J Cell Biochem*. 2010 Jul 1;110(4):935-47. doi: 10.1002/jcb.22607
13. Sun Y, Byon CH, Yuan K, Chen J, Mao X, Heath JM, Javed A, Zhang K, Anderson PG, Chen Y. Smooth muscle cell-specific runx2 deficiency inhibits vascular calcification. *Circ Res*. 2012 Aug 17;111(5):543-52. doi: 10.1161/CIRCRESAHA.112.267237
14. Boström KI. Where do we stand on vascular calcification? *Vascul Pharmacol*. 2016 Sep;84:8-14. doi: 10.1016/j.vph.2016.05.014
15. Ruffenach G, Chabot S, Tanguay VF, Courboulin A, Boucherat O, Potus F, Meloche J, Pflieger A, Breuils-Bonnet S, Nadeau V, Paradis R, Tremblay E, Girerd B, Hautefort A, Montani D, Fadel E, Dorfmuller P, Humbert M, Perros F, Paulin R, Provencher S, Bonnet S. Role for Runt-related Transcription Factor 2 in Proliferative and Calcified Vascular Lesions in Pulmonary Arterial Hypertension. Am J Respir Crit Care Med. 2016 Nov 15;194(10):1273-1285. doi: 10.1164/rccm.201512-2380OC
16. Liu TM, Lee EH. Transcriptional regulatory cascades in Runx2-dependent bone development. *Tissue Eng Part B Rev*. 2013 Jun;19(3):254-63. doi: 10.1089/ten.TEB.2012.0527
17. Dieffenbach PB, Haeger CM, Coronata AMF, Choi KM, Varelas X, Tschumperlin DJ, Fredenburgh LE. Arterial stiffness induces remodeling phenotypes in pulmonary artery smooth muscle cells via YAP/TAZ-mediated repression of cyclooxygenase-2. *Am J Physiol Lung Cell Mol Physiol*. 2017 Sep 1;313(3):L628-L647. doi: 10.1152/ajplung.00173.2017
18. Bertero T, Cottrill KA, Lu Y, Haeger CM, Dieffenbach P, Annis S, Hale A, Bhat B, Kaimal V, Zhang YY, Graham BB, Kumar R, Saggar R, Saggar R, Wallace WD, Ross

DJ, Black SM, Fratz S, Fineman JR, Vargas SO, Haley KJ, Waxman AB, Chau BN, Fredenburgh LE, Chan SY. Matrix Remodeling Promotes Pulmonary Hypertension through Feedback Mechanoactivation of the YAP/TAZ-miR-130/301 Circuit. *Cell Rep*. 2015 Nov 3;13(5):1016-32. doi: 10.1016/j.celrep.2015.09.049

19. Kudryashova TV, Goncharov DA, Pena A, Kelly N, Vanderpool R, Baust J, Kobir A, Shufesky W, Mora AL, Morelli AE, Zhao J, Ihida-Stansbury K, Chang B, DeLisser H, Tuder RM, Kawut SM, Silljé HH, Shapiro S, Zhao Y, Goncharova EA. HIPPO-Integrin-linked Kinase Cross-Talk Controls Self-Sustaining Proliferation and Survival in Pulmonary Hypertension. *Am J Respir Crit Care Med*. 2016 Oct 1;194(7):866-877. doi: 10.1164/rccm.201510-2003OC
20. Matsumoto Y, La Rose J, Kent OA, Wagner MJ, Narimatsu M, Levy AD, Omar MH, Tong J, Krieger JR, Riggs E, Storozhuk Y, Pasquale J, Ventura M, Yeganeh B, Post M, Moran MF, Grynpas MD, Wrana JL, Superti-Furga G, Koleske AJ, Pendergast AM, Rottapel R. Reciprocal stabilization of ABL and TAZ regulates osteoblastogenesis through transcription factor RUNX2. *J Clin Invest*. 2016 Dec 1;126(12):4482-4496. doi: 10.1172/JCI87802
21. Miranda MZ, Bialik JF, Speight P, Dan Q, Yeung T, Szászi K, Pedersen SF, Kapus A. TGF-β1 regulates the expression and transcriptional activity of TAZ protein via a Smad3-independent, myocardin-related transcription factor-mediated mechanism. *J Biol Chem*. 2017 Sep 8;292(36):14902-14920. doi: 10.1074/jbc.M117.780502
22. Zaiman AL, Podowski M, Medicherla S, Gordy K, Xu F, Zhen L, Shimoda LA, Neptune E, Higgins L, Murphy A, Chakravarty S, Protter A, Sehgal PB, Champion HC, Tuder RM. Role of the TGF-beta/Alk5 signaling pathway in monocrotaline-induced pulmonary hypertension. *Am J Respir Crit Care Med*. 2008 Apr 15;177(8):896-905. doi: 10.1164/rccm.200707-1083OC
23. Chen YF, Feng JA, Li P, Xing D, Zhang Y, Serra R, Ambalavanan N, Majid-Hassan E, Oparil S. Dominant negative mutation of the TGF-beta receptor blocks hypoxia-induced pulmonary vascular remodeling. *J Appl Physiol (1985)*. 2006 Feb;100(2):564-71. doi: 10.1152/japplphysiol.00595.2005
24. Graham BB, Chabon J, Gebreab L, Poole J, Debella E, Davis L, Tanaka T, Sanders L, Dropcho N, Bandeira A, Vandivier RW, Champion HC, Butrous G, Wang XJ, Wynn

TA, Tuder RM. Transforming growth factor-β signaling promotes pulmonary hypertension caused by Schistosoma mansoni. *Circulation*. 2013 Sep 17;128(12):1354-64. doi: 10.1161/CIRCULATIONAHA.113.003072

25. Zhang H, Huang W, Liu H, Zheng Y, Liao L. Mechanical stretching of pulmonary vein stimulates matrix metalloproteinase-9 and transforming growth factor-β1 through stretch-activated channel/MAPK pathways in pulmonary hypertension due to left heart disease model rats. *PLoS One*. 2020 Sep 3;15(9):e0235824. doi: 10.1371/journal.pone.0235824
26. Fujimoto Y, Urashima T, Kawachi F, Akaike T, Kusakari Y, Ida H, Minamisawa S. Pulmonary hypertension due to left heart disease causes intrapulmonary venous arterialization in rats. *J Thorac Cardiovasc Surg*. 2017 Nov;154(5):1742-1753.e8. doi: 10.1016/j.jtcvs.2017.06.053
27. Yin J, Kukucka M, Hoffmann J, Sterner-Kock A, Burhenne J, Haefeli WE, Kuppe H, Kuebler WM. Sildenafil preserves lung endothelial function and prevents pulmonary vascular remodeling in a rat model of diastolic heart failure. *Circ Heart Fail*. 2011 Mar;4(2):198-206. doi: 10.1161/CIRCHEARTFAILURE.110.957050
28. Hoffmann J, Yin J, Kukucka M, Yin N, Saarikko I, Sterner-Kock A, Fujii H, Leong-Poi H, Kuppe H, Schermuly RT, Kuebler WM. Mast cells promote lung vascular remodelling in pulmonary hypertension. *Eur Respir J*. 2011 Jun;37(6):1400-10. doi: 10.1183/09031936.00043310
29. Kerem A, Yin J, Kaestle SM, Hoffmann J, Schoene AM, Singh B, Kuppe H, Borst MM, Kuebler WM. Lung endothelial dysfunction in congestive heart failure: role of impaired Ca2+ signaling and cytoskeletal reorganization. *Circ Res*. 2010 Apr 2;106(6):1103-16. doi: 10.1161/CIRCRESAHA.109.210542.
30. Delgado C, Baweja M, Crews DC, Eneanya ND, Gadegbeku CA, Inker LA, Mendu ML, Miller WG, Moxey-Mims MM, Roberts GV, St Peter WL, Warfield C, Powe NR. A Unifying Approach for GFR Estimation: Recommendations of the NKF-ASN Task Force on Reassessing the Inclusion of Race in Diagnosing Kidney Disease. *J Am Soc Nephrol*. 2021 Dec 1;32(12):2994-3015. doi: 10.1681/ASN.2021070988.
31. Sang P, Kucherenko MM, Yao J, Li Q, Simmons S, Kuebler WM, Knosalla C. A Model of Reverse Vascular Remodeling in Pulmonary Hypertension Due to Left Heart Disease by Aortic Debanding in Rats. *J Vis Exp*. 2022 Mar 1;(181). doi: 10.3791/63502

32. Ott C, Pappritz K, Hegemann N, John C, Jeuthe S, McAlpine CS, Iwamoto Y, Lauryn JH, Klages J, Klopfleisch R, Van Linthout S, Swirski F, Nahrendorf M, Kintscher U, Grune T, Kuebler WM, Grune J. Spontaneous Degenerative Aortic Valve Disease in New Zealand Obese Mice. *J Am Heart Assoc*. 2021 Dec 7;10(23):e023131. doi: 10.1161/JAHA.121.023131
33. Zabini D, Granton E, Hu Y, Miranda MZ, Weichelt U, Breuils Bonnet S, Bonnet S, Morrell NW, Connelly KA, Provencher S, Ghanim B, Klepetko W, Olschewski A, Kapus A, Kuebler WM. Loss of SMAD3 Promotes Vascular Remodeling in Pulmonary Arterial Hypertension via MRTF Disinhibition. *Am J Respir Crit Care Med*. 2018 Jan 15;197(2):244-260. doi: 10.1164/rccm.201702-0386OC
34. Prasadam I, Friis T, Shi W, van Gennip S, Crawford R, Xiao Y. Osteoarthritic cartilage chondrocytes alter subchondral bone osteoblast differentiation via MAPK signalling pathway involving ERK1/2. *Bone*. 2010 Jan;46(1):226-35. doi: 10.1016/j.bone.2009.10.014
35. Chen P, Hong W, Chen Z, Gordillo-Martinez F, Wang S, Fan H, Liu Y, Dai Y, Wang B, Jiang L, Yu H, He P. CCAAT/Enhancer-Binding Protein Alpha Is a Novel Regulator of Vascular Smooth Muscle Cell Osteochondrogenic Transition and Vascular Calcification. *Front Physiol*. 2022 Feb 28;13:755371. doi: 10.3389/fphys.2022.755371
36. Kucherenko MM, Sang P, Yao J, Gransar T, Dhital S, Grune J, Simmons S, Michalick L, Wulsten D, Thiele M, Shomroni O, Hennig F, Yeter R, Solowjowa N, Salinas G, Duda GN, Falk V, Vyavahare NR, Kuebler WM, Knosalla C. Elastin stabilization prevents impaired biomechanics in human pulmonary arteries and pulmonary hypertension in rats with left heart disease. *Nat Commun*. 2023 Jul 21;14(1):4416. doi: 10.1038/s41467-023-39934-z
37. Lee KS, Kim HJ, Li QL, Chi XZ, Ueta C, Komori T, Wozney JM, Kim EG, Choi JY, Ryoo HM, Bae SC. Runx2 is a common target of transforming growth factor beta1 and bone morphogenetic protein 2, and cooperation between Runx2 and Smad5 induces osteoblast-specific gene expression in the pluripotent mesenchymal precursor cell line C2C12. *Mol Cell Biol*. 2000 Dec;20(23):8783-92. doi: 10.1128/MCB.20.23.8783-8792.2000

38. Takagi M, Kamiya N, Takahashi T, Ito S, Hasegawa M, Suzuki N, Nakanishi K. Effects of bone morphogenetic protein-2 and transforming growth factor beta1 on gene expression of transcription factors, AJ18 and Runx2 in cultured osteoblastic cells. *J Mol Histol*. 2004 Jan;35(1):81-90. doi: 10.1023/b:hijo.0000021151.31118.e3
39. Bertero T, Oldham WM, Cottrill KA, Pisano S, Vanderpool RR, Yu Q, Zhao J, Tai Y, Tang Y, Zhang YY, Rehman S, Sugahara M, Qi Z, Gorcsan J 3rd, Vargas SO, Saggar R, Saggar R, Wallace WD, Ross DJ, Haley KJ, Waxman AB, Parikh VN, De Marco T, Hsue PY, Morris A, Simon MA, Norris KA, Gaggioli C, Loscalzo J, Fessel J, Chan SY. Vascular stiffness mechanoactivates YAP/TAZ-dependent glutaminolysis to drive pulmonary hypertension. *J Clin Invest*. 2016 Sep 1;126(9):3313-35. doi: 10.1172/JCI86387
40. Gibault F, Bailly F, Corvaisier M, Coevoet M, Huet G, Melnyk P, Cotelle P. Molecular Features of the YAP Inhibitor Verteporfin: Synthesis of Hexasubstituted Dipyrrins as Potential Inhibitors of YAP/TAZ, the Downstream Effectors of the Hippo Pathway. *ChemMedChem*. 2017 Jun 21;12(12):954-961. doi: 10.1002/cmdc.201700063.
41. Buchanan BW, Lloyd ME, Engle SM, Rubenstein EM. Cycloheximide Chase Analysis of Protein Degradation in Saccharomyces cerevisiae. *J Vis Exp*. 2016 Apr 18;(110):53975. doi: 10.3791/53975
42. Kim MS, Gernapudi R, Choi EY, Lapidus RG, Passaniti A. Characterization of CADD522, a small molecule that inhibits RUNX2-DNA binding and exhibits antitumor activity. *Oncotarget*. 2017 Aug 10;8(41):70916-70940. doi: 10.18632/oncotarget.20200
43. Tanguay VF, Babin C, Giardetti G, Sohier-Poirier C, Ménard-Cholette V, Ranchoux B, Ruffenach G, Montani D, Bonnet S, Provencher S. Enhanced Pulmonary Artery Radiodensity in Pulmonary Arterial Hypertension: A Sign of Early Calcification? *Am J Respir Crit Care Med*. 2019 Mar 15;199(6):799-802. doi: 10.1164/rccm.201806-1027LE
44. Chuang KH, Yao RH, Jiang YN, Gui LX, Zheng SY, Lin MJ. Attenuating effect of magnesium on pulmonary arterial calcification in rodent models of pulmonary hypertension. *J Hypertens*. 2022 Oct 1;40(10):1979-1993. doi: 10.1097/HJH.0000000000003211

45. Mao M, Zhang M, Ge A, Ge X, Gu R, Zhang C, Fu Y, Gao J, Wang X, Liu Y, Zhu D. Granzyme B deficiency promotes osteoblastic differentiation and calcification of vascular smooth muscle cells in hypoxic pulmonary hypertension. *Cell Death Dis*. 2018 Feb 14;9(2):221. doi: 10.1038/s41419-018-0315-5
46. Sikura KÉ, Potor L, Szerafin T, Zarjou A, Agarwal A, Arosio P, Poli M, Hendrik Z, Méhes G, Oros M, Posta N, Beke L, Fürtös I, Balla G, Balla J. Potential Role of H-Ferritin in Mitigating Valvular Mineralization. *Arterioscler Thromb Vasc Biol*. 2019 Mar;39(3):413-431. doi: 10.1161/ATVBAHA.118.312191
47. Li W, Feng W, Su X, Luo D, Li Z, Zhou Y, Zhu Y, Zhang M, Chen J, Liu B, Huang H. SIRT6 protects vascular smooth muscle cells from osteogenic transdifferentiation via Runx2 in chronic kidney disease. *J Clin Invest*. 2022 Jan 4;132(1):e150051. doi: 10.1172/JCI150051
48. Bartoli-Leonard F, Wilkinson FL, Schiro A, Inglott FS, Alexander MY, Weston R. Suppression of SIRT1 in Diabetic Conditions Induces Osteogenic Differentiation of Human Vascular Smooth Muscle Cells via RUNX2 Signalling. *Sci Rep*. 2019 Jan 29;9(1):878. doi: 10.1038/s41598-018-37027-2
49. Lin ME, Chen TM, Wallingford MC, Nguyen NB, Yamada S, Sawangmake C, Zhang J, Speer MY, Giachelli CM. Runx2 deletion in smooth muscle cells inhibits vascular osteochondrogenesis and calcification but not atherosclerotic lesion formation. *Cardiovasc Res*. 2016 Nov 1;112(2):606-616. doi: 10.1093/cvr/cvw205
50. Wang L, Chennupati R, Jin YJ, Li R, Wang S, Günther S, Offermanns S. YAP/TAZ Are Required to Suppress Osteogenic Differentiation of Vascular Smooth Muscle Cells. *iScience*. 2020 Nov 26;23(12):101860. doi: 10.1016/j.isci.2020.101860
51. Liu-Chittenden Y, Huang B, Shim JS, Chen Q, Lee SJ, Anders RA, Liu JO, Pan D. Genetic and pharmacological disruption of the TEAD-YAP complex suppresses the oncogenic activity of YAP. *Genes Dev*. 2012 Jun 15;26(12):1300-5. doi: 10.1101/gad.192856.112
52. Wei C, Li X. Verteporfin inhibits cell proliferation and induces apoptosis in different subtypes of breast cancer cell lines without light activation. *BMC Cancer*. 2020 Oct 29;20(1):1042. doi: 10.1186/s12885-020-07555-0
53. Lui JW, Xiao S, Ogomori K, Hammarstedt JE, Little EC, Lang D. The Efficiency of Verteporfin as a Therapeutic Option in Pre-Clinical Models of Melanoma. *J Cancer*. 2019 Jan 1;10(1):1-10. doi: 10.7150/jca.27472

54. Woodside KH. Effects of cycloheximide on protein degradation and gluconeogenesis in the perfused rat liver. *Biochim Biophys Acta*. 1976 Jan 14;421(1):70-9. doi: 10.1016/0304-4165(76)90170-7
55. Nakajima H, Yamamoto K, Agarwala S, Terai K, Fukui H, Fukuhara S, Ando K, Miyazaki T, Yokota Y, Schmelzer E, Belting HG, Affolter M, Lecaudey V, Mochizuki N. Flow-Dependent Endothelial YAP Regulation Contributes to Vessel Maintenance. *Dev Cell*. 2017 Mar 27;40(6):523-536.e6. doi: 10.1016/j.devcel.2017.02.019
56. Damman K, Testani JM. The kidney in heart failure: an update. *Eur Heart J*. 2015 Jun 14;36(23):1437-44. doi: 10.1093/eurheartj/ehv010
57. Yu FX, Guan KL. The Hippo pathway: regulators and regulations. *Genes Dev*. 2013 Feb 15;27(4):355-71. doi: 10.1101/gad.210773.112
58. Dieffenbach PB, Maracle M, Tschumperlin DJ, Fredenburgh LE. Mechanobiological Feedback in Pulmonary Vascular Disease. *Front Physiol*. 2018 Jul 25;9:951. doi: 10.3389/fphys.2018.00951
59. Bessler NM; Vam Study Writing Committee. Verteporfin therapy in age-related macular degeneration (VAM): an open-label multicenter photodynamic therapy study of 4,435 patients. *Retina*. 2004 Aug;24(4):512-20. doi: 10.1097/00006982-200408000-00003
60. Gokey JJ, Sridharan A, Xu Y, Green J, Carraro G, Stripp BR, Perl AT, Whitsett JA. Active epithelial Hippo signaling in idiopathic pulmonary fibrosis. *JCI Insight*. 2018 Mar 22;3(6):e98738. doi: 10.1172/jci.insight.98738
61. Clark RAF. To Scar or Not to Scar. *N Engl J Med*. 2021 Jul 29;385(5):469-471. doi: 10.1056/NEJMcibr2107204

Statutory Declaration

I, Liu, Shaofei, by personally signing this document in lieu of an oath, hereby affirm that I prepared the submitted dissertation on the topic "TAZ-regulated RUNX2 signaling drives pulmonary artery calcification in pulmonary hypertension due to left heart disease (TAZ-reguliertes RUNX2-Signaling fördert die Verkalkung der Lungenarterie bei pulmonaler Hypertonie aufgrund von Links-herzerkrankungen)", independently and without the support of third parties and that I used no other sources and aids than those stated.
All parts which are based on the publications or presentations of other authors, either in letter or in spirit, are specified as such in accordance with the citing guidelines. The sections on methodology (in particular regarding practical work, laboratory regulations, and statistical processing) and results (in particular regarding figures, charts, and tables) are exclusively my responsibility.

Furthermore, I declare that I have correctly marked all of the data, the analyses, and the conclusions generated from data obtained in collaboration with other persons, and that I have correctly marked my own contribution and the contributions of other persons (cf. declaration of contribution). I have correctly marked all texts or parts of texts that were generated in collaboration with other persons.

My contributions to any publications to this dissertation correspond to those stated in the below joint declaration made together with the supervisor. All publications created within the scope of the dissertation comply with the guidelines of the ICMJE (International Committee of Medical Journal Editors; http://www.icmje.org) on authorship. In addition, I declare that I shall comply with the regulations of Charité – Universitätsmedizin Berlin on ensuring good scientific practice.

I declare that I have not yet submitted this dissertation in identical or similar form to another Faculty.

The significance of this statutory declaration and the consequences of a false statutory declaration under criminal law (Sections 156, 161 of the German Criminal Code) are known to me.

Date Signature

Curriculum Vitae

My curriculum vitae does not appear in the electronic version of my paper for reasons of data protection.

Publication list

1. **Shao-Fei Liu***, Mariya M. Kucherenko*, Pengchao Sang, Qiuhua Li, Juquan Yao, Netra Nambiar Veetil1, Tara Gransar, Ioana Alesutan, Jakob Voelkl, Szandor Simmons1, Christoph Knosalla# and Wolfgang M. Kuebler#. TAZ-regulated RUNX2 signaling drives pulmonary artery calcification in pulmonary hypertension due to left heart disease. **European Respiratory Journal. (IF=24.3, shared first-author, under revision).** * # equal author contribution.
2. Rui Zhang, Ji Zhang, Yun-Long Zhang, Su-Gang Gong, Qin-Hua Zhao, Xiao-Juan Wang, Jia-Yu Zhao, Rong Jiang, Hong-Ling Qiu, Hui-Ting Li, Jing He, **Shao-Fei Liu**, Wolfgang M Kuebler, Lan Wang. Single-Cell Transcriptome Analysis of Peripheral Neutrophils From Patients With Idiopathic Pulmonary Arterial Hypertension. **Hypertension.** 2023 Jun 14. (**IF=8.3, co-author**)
3. **Shao-Fei Liu***, Netra Nambiar Veetil*, Qiuhua Li, Mariya M. Kucherenko, Christoph Knosalla, Wolfgang M. Kuebler, Pulmonary Hypertension: Linking Inflammation and Pulmonary Arterial Stiffening. **Frontiers in Immunology, section Inflammation.** 2022 Oct 5;13:959209. (**IF=8.786, 1th shared co-author**). * equal author contribution.
4. Qi Zhang, Nobuhiro Yaoita, Arata Tabuchi, **Shaofei Liu**, Shiau-Haln Chen, Qiuhua Li, Niklas Hegemann, Caihong Li, Julie Rodor, Sara Timm, Hebatullah Laban, Toren Finkel, Troy Stevens, Diego F Alvarez, Lasti Erfinanda, Marc de Perrot, Mariya M Kucherenko, Christoph Knosalla, Matthias Ochs, Stefanie Dimmeler, Thomas Korff, Subodh Verma, Andrew H Baker, Wolfgang M Kuebler. Endothelial Heterogeneity in the Response to Autophagy Drives Small Vessel Muscularization in Pulmonary Hypertension. **Circulation**. 2024 Jun 14. (**IF=37.8, co-author**)
5. **Shao-Fei Liu**, Yi Yan. The animal model of Pulmonary Hypertension Due to Left Heart Disease. **Animal Model and Experimental Medicine.** 2022 Sep;5(3):197-206. **(IF=3.7,1st and Corresponding Author)**
6. Pengfei Liu, Aikai Zhang, Zheng Ding, Dongpu Dai, Boyan Li, **Shao-Fei Liu**, Jingjing Xu, Zhe Cheng, Song Zhao, Xiaoyan Zhao, Jianzeng Dong. m6A Modification-Mediated GRAP Regulates Vascular Remodeling in Hypoxic Pulmonary Hypertension. **American Journal of Respiratory Cell and Molecular Biology**. 2022 Aug 16. **(IF=6.4, co-author)**

7. Yan Liu, Jun-Zhuo Shi, Rong Jiang, **Shao-Fei Liu**, Yang-Yang He, Emiel van der Vorst, Christian Weber, Yvonne Döring, Yi Yan. Regulatory T cell-related gene indicators in pulmonary hypertension. **Frontiers in Pharmacology, section Experimental Pharmacology and Drug Discovery**. 2022 May 31;13:908783. **(IF=5.6, 4th Author)**
8. Xiao-Jian Wang, Tian-Yu Lian, Xin Jiang, **Shao-Fei Liu**, Su-Qi Li, Rong Jang, Wen-Hui Wu, Jue Ye, Chun-Yan Cheng, Yao Du, Xi-Qi Xu, Yan Wu, Fu-Hua Peng, Kai Sun, Yi-Min Mao, Huan Yu, Chen Liang, John Y-J. Shyy, Shu-Yang Zhang, Xue Zhang, Zhi-Cheng Jing. Germline BMP9 mutation causes idiopathic pulmonary arterial hypertension. **European Respiratory Journal.** 2019 53: 1801609. **(IF=24.3, 4th Author)**
9. Wen-Hui Wu, Ping Yuan, Si-Jin Zhang, Xin Jiang, Cheng Wu, Yuan Li, **Shao-Fei Liu**, Qian-Qian Liu, Jing-Hui Li, Bigyan Pudasaini, Qing-Hua Hu, Jocelyn Dupuis, and Zhi-Cheng Jing. Impact of Pituitary–Gonadal Axis Hormones on Pulmonary Arterial Hypertension in Men. **Hypertension.** 2018;72:151–158. (**IF=8.3, co-author**)
10. Zi-Chao Lyu, Lan Wang, Jian-Hui Lin, Su-Qi Li, Danchen Wu, Tian-Yu Lian, **Shao-Fei Liu**, Jue Ye, Xin Jiang, Xiao-Jian Wang, Zhi-Cheng Jing. The Features of Rare Pathogenic BMPR2 Variants in Pulmonary Arterial Hypertension: Comparison Between Patients and Reference Population. **International Journal of Cardiology.** 2020; 318:138-143. (**IF=4.0, co-author**)
11. 刘少飞,匡雅姝,彭盛,闫建设,李莹.单核细胞来源的微颗粒通过 PPAR-α -SR-BI 途径促进 RAW264.7 泡沫细胞形成的研究.同济大学学报(医学版),2017,(4):6-12. (**1st Author**)
12. 张汝姣,何阳阳,姜栋,刘少飞, 张宇佳,郑稳生,吴松,荆志成.高效液相色谱串联质谱法测定大鼠血浆中伐地那非浓度的可行性研究.《中华心血管病杂志》, 2020 年第 6 期 507-512. (**co-Author**)

Acknowledgments

I have embarked on a remarkable journey to pursue my doctoral thesis and as I reflect upon every step of my studies and life in Berlin, I am overwhelmed with gratitude towards those who have supported me along the way. First and foremost, I would like to express my deepest appreciation to my parents for their unwavering support throughout this endeavor. Their encouragement and belief in my abilities have been invaluable.

I am immensely grateful to my supervisors for their guidance and assistance in shaping my research project. Their expertise and mentorship have been instrumental in my academic and personal growth. I would like to extend my heartfelt thanks to my friends who have provided assistance during my experiments, their collaboration and camaraderie have made this journey even more meaningful.

I am indebted to my home country for providing the necessary funds that have made it possible for me to pursue my studies in Berlin. The financial support has been crucial in enabling me to complete my education here, and I am grateful for this opportunity.

A special note of gratitude goes to my advisor, Prof. Wolfgang M. Kuebler, whose research design and invaluable suggestions have played a pivotal role in shaping the trajectory of my thesis. Without his exceptional guidance, patience, and expertise, this thesis would not have attained its current form. The memory of our first meeting in London in 2014 is etched deeply in my mind, and I doubt I will ever forget it. It marked the beginning of a journey that has shaped our fate and brought us together.

I express my sincere gratitude to Mariya Kucherenko and Szandor Simmons for their dedicated supervision of animal studies. Their guidance and expertise have been invaluable in successfully conducting our experiments. Special acknowledgment goes to Qiuhua Li, Juquan Yao, and Pengchao Sang, whose skillful execution of surgical procedures, echocardiography, and final cardiac catheterization greatly contributed to our research. Furthermore, I extend my thanks to Christoph Knosalla, Mariya Kucherenko, Netra Veetil, and Tara Gransar from DHZC for their assistance in collecting clinical information, phenotyping human biomaterials, and their involvement in the isolation of primary PASMC. Gratitude is also owed to our collaborators, Ioana Alesutan and Jakob Voelkl from the Institute of Physiology and Pathophysiology at Johannes Kepler University Linz,

for their meticulous work in conducting calcium content measurements. A special appreciation is reserved for Dr. Mariya Kucherenko for her exceptional contributions to RNA sequencing and transcriptomics analysis. Her expertise and dedication have provided invaluable insights into our research findings. Their collective efforts have been pivotal in obtaining the necessary samples for our research.

To all my Chinese colleagues, espacilly Qi Zhang, Qiuhua Li, Caihong Li, Pengchao Sang, Juquan Yao and Mei Li, I extend my heartfelt thanks for their encouragement and support throughout these years. Their presence has made the academic environment vibrant and inspiring.

Finally, I would like to acknowledge the unwavering support of my family and friends. Their love, understanding, and encouragement have been my pillar of strength during this almost four-year journey abroad. I am forever grateful for everything they have done for me.

Statistician confirmation

CHARITÉ

CharitéCentrum für Human- und Gesundheitswissenschaften

Charité | Campus Charité Mitte | 10117 Berlin

Institut für Biometrie und klinische Epidemiologie (iBikE)

Direktor: Prof. Dr. Frank Konietschke

Postanschrift:
Charitéplatz 1 | 10117 Berlin
Besucheranschrift:
Reinhardtstr. 58 | 10117 Berlin

Tel. +49 (0)30 450 562171
frank.konietschke@charite.de
https://biometrie.charite.de/

Name, Vorname: Shaofei Liu
Emailadresse: Shaofei.liu@charite.de
Matrikelnummer:228961
PromotionsbetreuerIn: Wolfgang Kuebler
Promotionsinstitution / Klinik: The institute of physiology

Bescheinigung

Hiermit bescheinige ich, dass Herr *Shaofei Liu* innerhalb der Service Unit Biometrie des Instituts für Biometrie und klinische Epidemiologie (iBikE) bei mir eine statistische Beratung zu einem Promotionsvorhaben wahrgenommen hat. Folgende Beratungstermine wurden wahrgenommen:

- Termin 1: 24.01.2023

Folgende wesentliche Ratschläge hinsichtlich einer sinnvollen Auswertung und Interpretation der Daten wurden während der Beratung erteilt:

- Überprüfung der Normalverteilung
- Pearsonsche Korrelation und Spearmansche Rangkorrelation
- Analyse der Varianz
- Lineare Regression

Diese Bescheinigung garantiert nicht die richtige Umsetzung der in der Beratung gemachten Vorschläge, die korrekte Durchführung der empfohlenen statistischen Verfahren und die richtige Darstellung und Interpretation der Ergebnisse. Die Verantwortung hierfür obliegt allein dem Promovierenden. Das Institut für Biometrie und klinische Epidemiologie übernimmt hierfür keine Haftung.

Datum: 26.01.2023

Unterschrift BeraterIn, Institutsstempel